National Library of Canada
Acquisitions and Bibliographic Services Branch
395 Wellington Street
Ottawa, Ontario
K1A 0N4

Bibliothèque nationale du Canada
Direction des acquisitions et des services bibliographiques
395, rue Wellington
Ottawa (Ontario)
K1A 0N4

Your file Votre référence

Our file Notre référence

NOTICE

The quality of this microform is heavily dependent upon the quality of the original thesis submitted for microfilming. Every effort has been made to ensure the highest quality of reproduction possible.

If pages are missing, contact the university which granted the degree.

Some pages may have indistinct print especially if the original pages were typed with a poor typewriter ribbon or if the university sent us an inferior photocopy.

Reproduction in full or in part of this microform is governed by the Canadian Copyright Act, R.S.C. 1970, c. C-30, and subsequent amendments.

AVIS

La qualité de cette microforme dépend grandement de la qualité de la thèse soumise au microfilmage. Nous avons tout fait pour assurer une qualité supérieure de reproduction.

S'il manque des pages, veuillez communiquer avec l'université qui a conféré le grade.

La qualité d'impression de certaines pages peut laisser à désirer, surtout si les pages originales ont été dactylographiées à l'aide d'un ruban usé ou si l'université nous a fait parvenir une photocopie de qualité inférieure.

La reproduction, même partielle, de cette microforme est soumise à la Loi canadienne sur le droit d'auteur, SRC 1970, c. C-30, et ses amendements subséquents.

Canada

Al-Fe-Si INTERMETALLICS IN 1000 SERIES ALUMINUM ALLOYS

Gail Stephen

Department of Mining and Metallurgical Engineering
McGill University
Montreal, Canada

May 1994

A Thesis submitted to the Faculty of
Graduate Studies and Research
in partial fulfilment of
the requirements of the degree of
Master of Engineering

ISBN 0-315-99983-7

Canada

To my wonderful fiance Mireno...

ABSTRACT

Iron and silicon are the major impurities in the 1000 series of wrought aluminum alloys. As the aluminum is recycled, it picks up more and more of these impurities which cannot economically be refined out of the aluminum. When the concentration of these impurities reaches a certain limit (maximum limit in 1000 series is 1 weight percent (Fe+Si)), the aluminum must be downgraded. The Fe and Si form brittle intermetallic phases in these alloys. The two main phases are the plate-like β-AlFeSi (Al_5FeSi) and α-AlFeSi (Al_8Fe_2Si) which has a Chinese Script morphology. The mechanical properties of these alloys are believed to depend largely on the nature of these intermetallics.

In the first part of this study, the conditions at which the intermetallics form, along with the ability of strontium to modify them were investigated. The second part consisted of determining how the morphology of the Al-Fe-Si phases affects the mechanical properties of the worked product. It was found that the formation of the Chinese Script morphology is promoted with increasing cooling rates, Fe/Si ratios and additions of strontium. However, the relative amount of Chinese Script was found to decrease with increasing (Fe+Si) levels. Tensile testing and formability testing (Erichsen ball punch deformation test) revealed that the presence of a Chinese Script morphology of Al-Fe-Si intermetallics (as opposed to the plate-like morphology) imparts no significant beneficial effect on the formability of the final rolled sheet.

RESUME

Le fer et le silicium sont les impuretés majeures des alliages corroyés d'aluminium de la classe 1000. Lorsque l'aluminium est recyclé, il collecte de plus en plus de ces impuretés qui ne peuvent pas être éliminées économiquement de l'aluminium. Quand la concentration de ces impuretés atteint une certaine limite (la limite maximum dans la classe 1000 est de 1% en poids (Fe+Si)), l'aluminium doit être déclassé. Le fer et le silicium forment des phases intermétalliques fragiles dans ces alliages. Les deux phases principales sont β-AlFeSi (Al_5FeSi) en forme de plaques et α-AlFeSi (Al_8Fe_2Si) qui présente une morphologie de "Chinese Script". On pense que les propriétés mécaniques de ces alliages peuvent être largement dépendantes de la nature de ces intermétalliques.

Dans la première partie de cette étude, les conditions auxquelles les intermétalliques se forment, ainsi que l'habilité du strontium à les modifier ont été étudiées. La deuxième partie a porté sur l'influence de la morphologie des phases Al-Fe-Si sur les propriétés mécaniques du produit travaillé. Il a été trouvé que la formation de la morphologie "Chinese Script" est encouragée par des augmentations des vitesses de refroidissement, des ratios Fe/Si et par des additions de strontium. Cependant, la quantité relative de "Chinese Script" diminue avec des niveaux de (Fe+Si) plus élevés. Les essais de traction et d'aptitude au formage (essai de déformation Erichsen) ont révélé que la présence des intermétalliques Al-Fe-Si sous forme de "Chinese Script" (par opposition aux intermétalliques en plaques) n'apporte aucun effet bénéfique significatif pour la formabilité du produit final laminé.

ACKNOWLEDGEMENTS

I would like to express my sincere gratitude to Prof. J.E. Gruzleski for his supervision and encouragement throughout the course of this thesis.

I would like to thank Dr. M.H. Mulazimoglu and Dr. F. Paray for their advice and help during the course of this research, and a special thanks goes to Dr. F. Paray for translating the abstract.

I would also like to thank Mr. R. Paquette for his kind help in the foundry.

Further thanks goes to Mr. C. Edovas for this continuous help in the laboratories.

Finally, I would like to thank Mr. J. Akkermann and Alcan Kingston Research & Development Centre for the rolling of my samples and use of their equipment.

TABLE OF CONTENTS

Page

Page

LIST OF FIGURES

Page

LIST OF TABLES

Page

CHAPTER
1

INTRODUCTION

The aluminum industry offers a wide range of alloys with various combinations of mechanical strength, ductility, electrical conductivity and corrosion-resistance. These alloys can be divided into two main classifications, casting alloys and wrought alloys. The term "wrought" refers to certain aluminum alloys which are primarily available in the form of worked products, such as sheet, foil, plate, extrusions, tube, forgings, rod, bar and wire. The various wrought alloys are further divided into two basic classes: non-heat-treatable (i.e. 1000, 3000, 4000 and 5000 series) and heat-treatable (i.e. 2000, 6000 and 7000 series).

Many metals and combinations of metals are used to alloy aluminum. For example, a small addition of manganese increases the strength of wrought aluminum. Additions of magnesium and/or silicon produce alloys with good corrosion-resistance and strengths in the order of those of mild steels. Small quantities of other elements such as chromium, titanium , nickel and tin are often added for grain-refinement or to impart special characteristics.

When no alloying elements have been added to the aluminum, the resultant metal may still be considered as an alloy due to the small percentages of elements present as

impurities which have to be carefully controlled. The most common of these "alloys" contain 99.0 to 99.5 percent aluminum with the remainder being mainly iron and silicon. These two elements are difficult to economically refine out of the aluminum with the existing electrolytic technology, available today. When superior electrical conductivity or corrosion-resistance is desired, metal with over 99.5 percent aluminum content is required which can be obtained with additional refining. This group of "alloys" which consists of aluminum of 99 percent or higher purity makes up the 1000 series of wrought aluminum alloys.

As mentioned, the main impurities in the 1000 series are iron and silicon. These elements form second-phase particles, usually intermetallic phases of the Al-Fe or Al-Fe-Si type. These phases are formed as primary particles during the casting of aluminum and constitute an important part of the microstructure. These particles formed during solidification may influence the material properties during subsequent fabrication steps. Therefore, the ability to control the formation of Al-Fe-Si intermetallic phases in aluminum is of considerable technological importance.

This study deals with the Al-Fe-Si intermetallic phases which form in the 1000 series of wrought aluminum alloys. The conditions at which the different phases form along with the capability for strontium additions to promote certain phases are investigated in the first part of the study. The second part is an attempt to relate the as-cast microstructure of these alloys to the final mechanical properties of the worked product.

CHAPTER
2

LITERATURE REVIEW

2.1 1000 SERIES WROUGHT ALUMINUM ALLOYS

2.1.1 Chemical Composition and Major Impurities

The 1000 series of alloys consists of aluminum of 99 percent or higher purity. These alloys contain no major alloying elements and are often referred to as commercially pure aluminum. The major impurities in these alloys are iron and silicon. Their total concentration can be as high as 1 weight percent. Table 2.1 lists the chemical composition limits for some commercial 1000 series wrought alloys registered with the Aluminum Association.

Table 2.1 Chemical Composition Limits of 1000 Series Alloys (wt%)[1]

AA Desig-nation	Si	Fe	Cu	Mn	Zn	Ti	Al (min)
1050	0.25	0.40	0.05	0.05	0.05	0.03	99.50
1060	0.25	0.35	0.05	0.03	0.05	0.03	99.60
1100	0.95 Si+Fe		0.05-0.20	0.05	0.10	-	99.00
1145	0.55 Si+Fe		0.05	0.05	0.05	0.03	99.45
1175	0.15 Si+Fe		0.10	0.02	0.04	0.02	99.75
1200	1.00 Si+Fe		0.05	0.05	0.10	0.05	99.00
1230	0.70 Si+Fe		0.10	0.05	0.10	0.03	99.30
1235	0.65 Si+Fe		0.05	0.05	0.10	0.06	99.35
1345	0.03	0.40	0.10	0.05	0.05	0.03	99.45
1350	0.10	0.40	0.05	0.01	0.05	-	99.50

Iron is the most common impurity found in aluminum. It is a natural impurity in most aluminum ore bodies (bauxite). Iron pick-up can also occur in foundry processing from melting equipment such as ladles and holding furnace pots, and from recycled scrap metal. Iron has a high solubility in liquid aluminum and thus readily dissolves at all molten stages of production. The rate of iron dissolution increases with increasing melt temperature and decreases with increasing iron content in the molten aluminum bath. In solid state aluminum however, iron has a very low solubility (approximately 0.04 weight percent). Therefore, most of the iron present in aluminum appears as an intermetallic second phase in combination with aluminum and often other elements.

Silicon, after iron, has the highest impurity level (0.01 to 0.15 weight percent) in electrolytic commercial aluminum. Silicon pick-up comes mainly from recycled scrap aluminum metal. The iron and silicon impurities form brittle ternary Al-Fe-Si intermetallic phases which are considered detrimental to the mechanical and physical properties. Iron and silicon cannot be economically refined out of aluminum with the current electrolysis technology. Therefore every time the metal is recycled, it picks up more and more of these impurities and eventually must be downgraded.

Copper is the most common impurity after iron and silicon (0.05- 0.1 weight percent). Higher amounts of copper (up to 0.20 weight percent) are added to alloy 1100 to increase strength through solid solution, however there is a decrease in corrosion resistance and electrical conductivity.

Manganese is a common impurity (5-50 ppm) in primary aluminum. In commercial purity aluminum, manganese increases strength in solid solution and decreases resistivity. Manganese has a very limited solubility in aluminum, but remains in solution when chill cast so that most of the manganese added is substantially retained in solution [2].

Small amounts of **titanium** (10-100 ppm) are found in commercial purity aluminum. It depresses the electrical conductivity of aluminum, however its level can be reduced by adding boron to form insoluble TiB_2. Titanium is primarily added as a grain refiner to aluminum castings and ingots [2].

In the wrought condition, the addition of **zinc** to commercial purity aluminum yields only a modest improvement in strength. However, the presence of zinc increases the solution potential of aluminum, hence its use in protective cladding and in sacrificial anodes [2].

2.1.2 Mechanical Properties

The 1000 series compositions are characterized by excellent corrosion resistance, high thermal and electrical conductivity, low mechanical properties and excellent workability. These alloys are non-heat-treatable, however moderate increases in strength can be obtained by strain-hardening. Table 2.2 lists typical mechanical properties of some 1000 series alloys in both the annealed condition (O temper) as well as in a work-hardened state (H18 temper).

Table 2.2 Typical Mechanical Properties of 1000 Series Alloys[2]

Alloy	Temper[a]	Tensile Strength (MPa)	Yield Strength[b] (MPa)	Elongation in 50 mm (%)	Hardness (BHN)[c]
1060	O H18	70 130	30 125	43 6	19 35
1100	O H18	90 165	35 150	35 5	23 44
1145	O H18	75 145	35 115	40 5	...
1350	O H18	85 185	30 165	23[d] 2.5[d]	...

(a) O temper = fully annealed
H18 temper = 75% cold reduction after full anneal
(b) Yield Strength, 0.2% offset.
(c) 500 kg (1102 lb) load, 10 mm (0.4 in) ball, 30 s.
(d) Elongation in 250 mm (10 in).

The tensile properties of the various grades of commercial purity aluminum do not cover a very extensive range in strength in comparison to other alloy series which contain major alloying elements. For alloys with approximately the same aluminum content, only minor variations in strength occur. Often there is no change in strength and the control of the composition is related to other characteristics required for specific applications, such as conductivity or corrosion resistance.

2.1.3 Applications of 1000 Series Alloys

Commercially pure wrought products have many applications, especially in the packaging, chemical, electrical and architectural fields. Alloys containing up to 0.5 percent iron as a principal alloying element are used for applications requiring high

electrical conductivity. Alloy 1350, which has a minimum aluminum content of 99.50 percent, is the pure aluminum wrought material used today for electrical conductors. The aluminum used for commercial and household foil varies in purity from 98.6 to 99.9 percent aluminum. Another important application of pure aluminum is as cladding for other aluminum alloys to either protect them from corrosive influences, or to improve surface finishing by bright anodizing.

2.2 IRON AND SILICON IN ALUMINUM

2.2.1 Equilibrium Al-Fe-Si System

The Al-Fe-Si system is bordered by the Al-Fe, Al-Si and Fe-Si binary systems. Several intermetallic phases are known to exist in the binary Al-Fe and Fe-Si systems, however no intermetallic compound is formed in the Al-Si system. In aluminum-based ternary alloys, iron and silicon form ternary phases with aluminum and binary Fe-Si phases are never to be found. Since this study is concerned primarily with alloys which are near in composition to commercial pure aluminum (1000 series), the literature review will be limited to the binary Al-Fe and ternary Al-Fe-Si phases which are found in alloys with iron and silicon contents not higher than about 1 weight percent.

The most frequently used Al-Fe-Si phase diagram, the one suggested by Phillips (in 1943), is redrawn in figure 2.1. This diagram also includes other invariant points suggested by other scientists. These ternary elements produce four primary phase fields, namely: aluminum (α-Al), Al_3Fe, α-AlFeSi and β-AlFeSi.

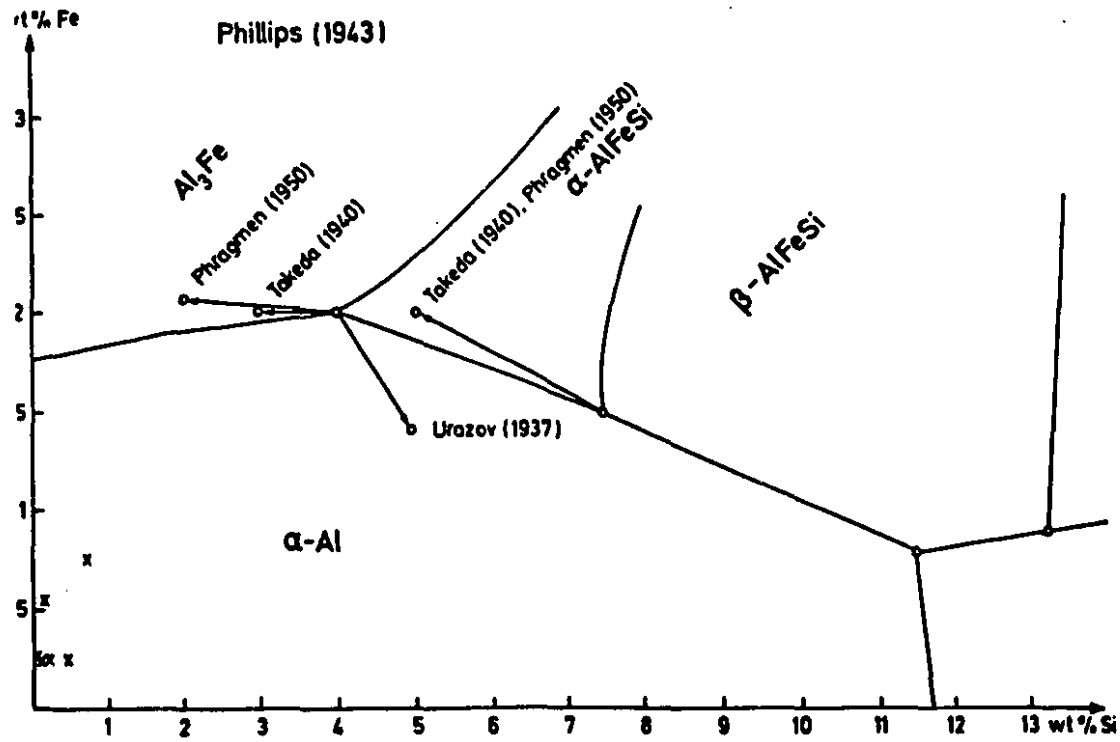

Figure 2.1 AlFeSi liquidus surface as suggested by Phillips[3]

The monoclinic Al_3Fe phase is considered as the only binary Al-Fe equilibrium intermetallic phase in alloys containing up to about 40 at% Fe [4]. The Al_3Fe phase crystallizes in the form of long prisms or needles. The Al_3Fe crystals form pseudo-tetragonal blades (plate-like morphology) for which the dominating faces belong to the {100} group. The binary compound appears mostly in alloys containing less than approximately 0.5 percent silicon.

The ternary α-AlFeSi equilibrium phase has a cubic symmetry with a varying composition range. The most commonly reported chemical formula corresponds to Al_8Fe_2Si [5]. The α-AlFeSi phase is also often reported as $Al_{12}Fe_3Si$ [6]. In a eutectic with solid aluminum, the α-AlFeSi crystals are constrained to interdendritic regions due to growth kinetic differences between the two phases. The α-AlFeSi phase forms strongly curved crystals which in some places grow together into plates with irregular, curved surfaces [7]. This spatial morphology appears in section as the well-known "Chinese Script" morphology, as shown in figure 2.2.

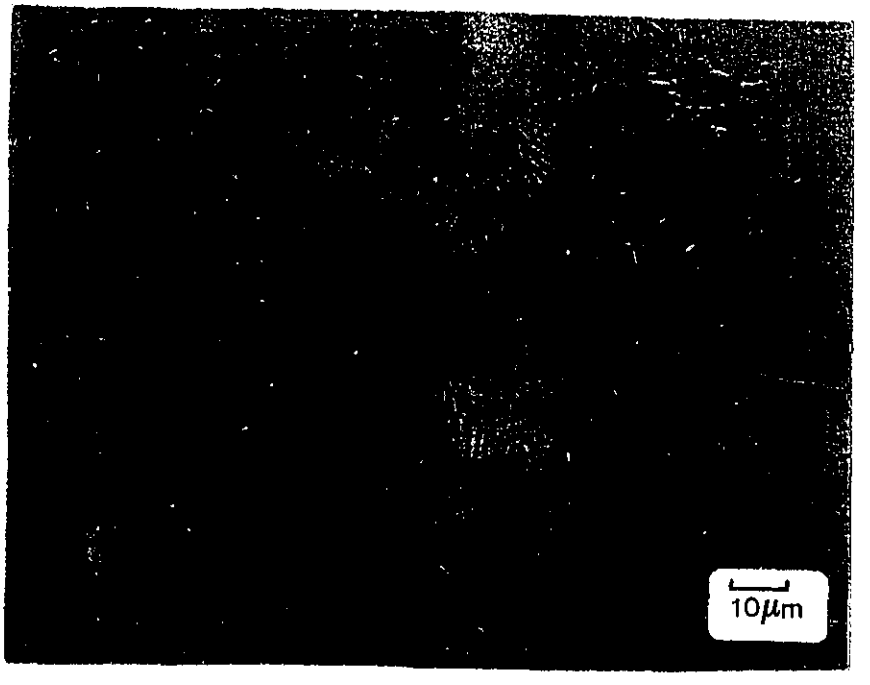

Figure 2.2 α-AlFeSi Chinese Script Intermetallic

The ternary β-AlFeSi phase has a monoclinic structure with a chemical formula approximating Al_5FeSi [6]. The β-AlFeSi crystals form pseudo-tetragonal blades in which the dominating faces belong to the {001} group. The crystals form twin lamellae for which the twinning planes belong to the {011} group. This β-AlFeSi phase, which crystallizes as very thin platelets, can be observed as needles on a flat polished surface. The microstructure of the β-AlFeSi phase is shown in figure 2.3.

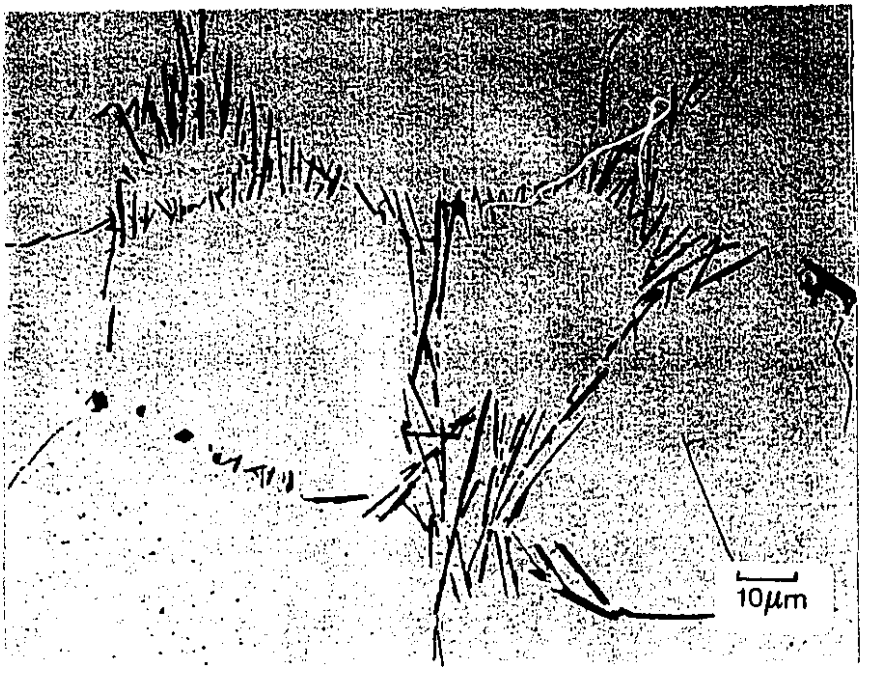

Figure 2.3 Acicular β-AlFeSi Intermetallic

2.2.2 Non-Equilibrium Al-Fe-Si System

Both iron and silicon combine with aluminum to form a series of intermetallic compounds, as described in the previous section. Since the solubility of iron and silicon in aluminum varies with cooling rate, the distribution of the elements in the as-cast structure greatly depends on the cooling rate upon solidification. As an example, several weight percent of iron and silicon can be retained in solid solution in castings that are rapidly solidified (splat quenching) [5]. However, commercial casting methods, such as sand or permanent mold casting, produce materials in which most of the iron, and to a certain degree the silicon, are present as intermetallic compounds in the interdendritic regions.

In industrial casting techniques, such as the Direct Chill semi-continuous process, wide differences in cooling conditions prevail from the centre to the outside of the ingots (0.5 to 10 K/s). In this case, the information contained in equilibrium phase diagrams may not necessarily be useful for predicting precipitation of second phases. Generally, phase diagrams are constructed from data obtained from experiments in which two or three very pure elements are given time to reach equilibrium at a given temperature. In industry however, alloys are cooled much faster and usually contain many other minor elements.

Furthermore, in order to be able to apply the Al-Fe-Si phase diagram to industrially cast alloys, a certain temperature which approaches equilibrium must be assumed. This temperature can be chosen as room temperature, the solidus temperature or some intermediate temperature, however different results can be obtained with

different assumptions. Another complication which can arise is that the alloy may contain certain alloying/impurity elements. These elements can possibly stabilize phases other than those indicated in the phase diagram. The presence of these minor elements along with high cooling rates favour the formation of metastable phases which are not predicted by the phase diagram. Also, the local cooling rate varies from the centre to the surface of the casting and therefore different Al-Fe-Si phases may form throughout the casting and phase distribution gradients may be introduced.

Since equilibrium phase diagrams are not very useful for predicting the precipitation of metastable phases, Dons [8] created a "particle diagram" as shown in figure 2.4, based on literature data and her results. This "particle diagram" gives a rough estimate of the phases that may form under the high cooling rates encountered in strip casting (approx. 10°C/s). However, this diagram is greatly dependent on the minor alloying/impurity elements as well as the local cooling rate.

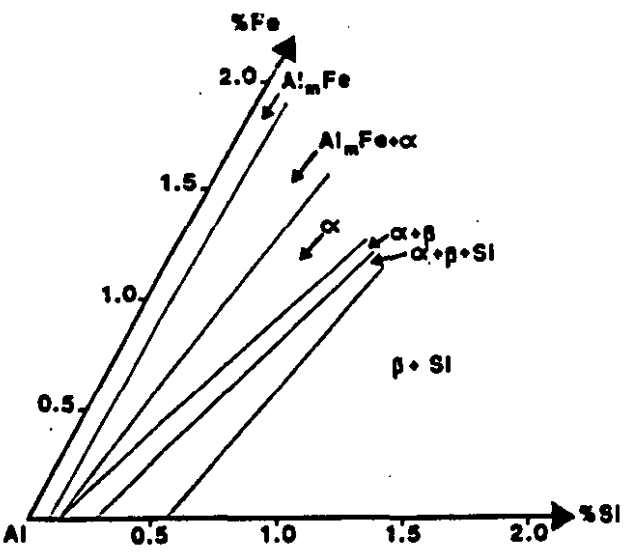

Figure 2.4 "Particle diagram" of strip casting[8]

Langsrud [3] suggested that in order to predict second phases, metastable phase diagrams have to be created, by shifting the phase boundaries in fig.2.1 and introducing phase fields for metastable phases. From his experimental work, Langsrud [3] proposed metastable phase diagrams for "high" (~10°C/s after complete solidification), "intermediate" (~3°C/s) and "low" (~1°C/s) cooling rates in DC-casting, as shown in figure 2.5.

Table 2.3 lists the intermetallic phases observed in industrially cast commercial pure aluminum along with their structures and lattice parameters.

Table 2.3 Intermetallic phases in commercial pure aluminum[4]

Name	Structure	a (nm)	b (nm)	c (nm)	β (°)
Al_3Fe	monoclinic	1.55	0.808	1.247	107
Al_6Fe	orthorhombic	0.649	0.744	0.879	-
Al_mFe	body centered tetragonal	0.884	1.25	-	-
Al_xFe	monoclinic	2.16	0.93	0.905	94
α	body centered cubic	1.256	-	-	-
α'	hexagonal	1.23	-	2.62	-
α''	tetragonal	1.26	-	3.70	-
α_v	monoclinic	0.847	0.635	0.610	93.4
α_T	monoclinic	2.81	3.08	4.156	97.74
β	monoclinic	0.612	0.612	4.156	91
β'	monoclinic	0.89	0.49	4.16	92

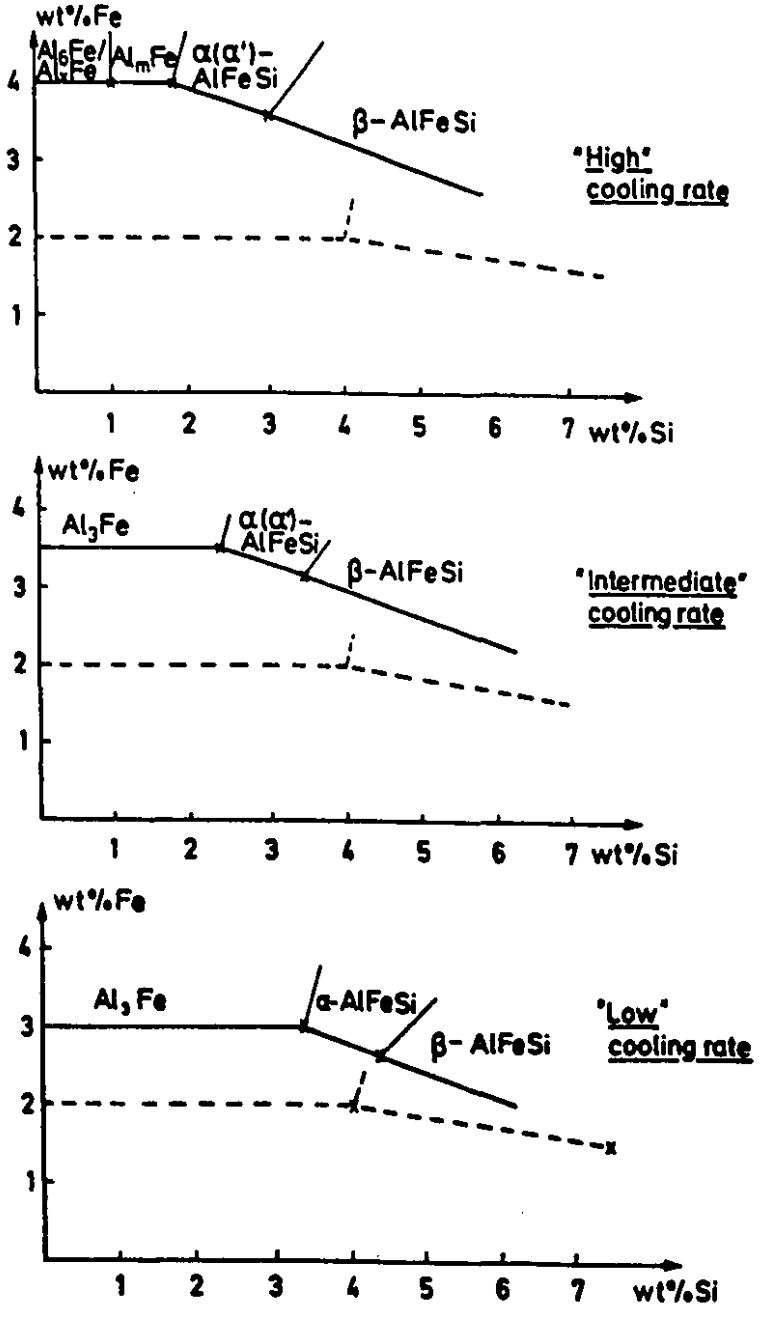

Figure 2.5 Suggested "metastable" Al-Fe-Si liquidus surfaces[3]

2.2.2.1 Binary Al-Fe Phases

The Al_3Fe intermetallic is the only binary Al-Fe phase that is reported to be an equilibrium phase. Miki et al [9] along with Young and Clyne [10] agree that Al_3Fe forms only at cooling rates less than 1 K/s. Hollingsworth et al [11] reported a metastable phase which was assigned the chemical formula Al_6Fe due to its close relationship to $MnAl_6$. The metastable Al_6Fe phase is reported to form at cooling rates of 1 to 10 K/s while the Al_mFe (value of m is approximately 4.4) is reported to form at cooling rates exceeding 10 K/s [10,12,13]. Finally, another binary Al-Fe metastable phase which has very irregular diffraction patterns was reported by Westengen [14] and termed Al_xFe (where x approximates 5.8). There is a general agreement [15,16] that Al_6Fe and Al_mFe (and possibly Al_xFe) transform to the more stable equilibrium phase Al_3Fe during annealing treatment at high temperatures (590°C).

2.2.2.2 Ternary Al-Fe-Si Phases

As seen in table 2.3, there are many variations of the α-AlFeSi phase. Dons [8] tried to sort out the different α-phases (i.e. phases with compositions in the range of $Al_{12-15}Fe_3Si_{1-2}$) according to the cooling rate when they are formed. They form under the following conditions:

Heat treatment: α, α', α'', α_T
DC cast, inner zone: α, α_v, α_T
DC cast, outer zone: α, α''
Strip cast: α

The **cubic α-AlFeSi phase** does not form in the pure ternary Al-Fe-Si system, however it can be stabilized by transition elements which are commonly present in commercial alloys such as manganese and chromium [15,17]. Since α is a less ordered phase than α', it is expected to be favoured by rapid cooling [8]. It may develop one of the superstructures α'' or α_T at intermediate cooling rates or after heat treatment.

In the absence of transition elements other than iron, the **hexagonal α'-AlFeSi phase** is regarded as the equilibrium form of α [17]. This α' phase is difficult to nucleate and is generally observed after heat treatment [8]. Sun and Mondolfo [15] reported that the α' phase can also form in the pure Al-Fe-Si system.

The **α''-AlFeSi phase**, which has a tetragonal crystal structure that is closely related to that of the cubic α, has been reported in certain alloys [14]. Since two axes are identical and the third is roughly multiplied by a factor of three, basically 3 unit cells of the cubic α constitute 1 unit cell of the α'' phase.

Siemensen and Vellasamy [16] reported a **new phase, α_V-AlFeSi**, which is structurally related to the Al_9Fe_2 phase. Both the a and c axes are shorter than in Al_9Fe_2 and the composition also differs. Dons [18] reported silicon contents of 4.5-10.5 percent, while Al_9Fe_2 contains less than 2 percent silicon. This composition falls within the α-α' range and the structure was named α_V after Vellasamy.

Dons [18] reported a new ternary phase (**α_T-AlFeSi**) which is similar in composition to α-AlFeSi, however it had larger variations in Fe and Si content than the BCC α phase. This new phase has diffraction patterns similar to those of α-AlFeSi except for a few extra diffraction spots.

The **monoclinic β-AlFeSi phase** is observed in alloys containing more than 1% silicon. In alloys containing less than 1 percent silicon, the **β'-AlFeSi phase** is observed. The β'-AlFeSi phase shows some resemblance to the well-known β-AlFeSi phase [14], but with slightly different lattice parameters (see table 2.3).

2.2.3 Growth of Intermetallics

Griger et al [7] divided the intermetallic phases into two types according to their micromorphology. The first group consists of Al_3Fe and β-AlFeSi. The crystal form of these phases shows lateral or faceted growth. These type of crystals are bounded by slowly growing planes of low indices. These surfaces are relatively "smooth" on the atomic scale. Therefore, atoms from the liquid have few possibilities to join the interface and thus growth is restricted and slow.

The second group consists of phases that grow continuously (i.e. normally). The Al_6Fe, Al_mFe and α-AlFeSi phases belong to this group on the basis of their morphology. These phases grow in irregular, curved crystal form conforming to the complicated shape of the interdendritic regions upon solidification. Atoms are able to add on to the solidified part upon arrival at the interface during crystallization. In this case, the interface between the solid and the liquid is "rough". The temperature gradient and the diffusion of atoms in the liquid control the form of the crystals.

2.3 EFFECT OF INTERMETALLICS ON PROPERTIES

Very little experimental work dealing with the effect of Al-Fe-Si intermetallics on the mechanical properties of wrought aluminum alloys has been published. However, literature dealing with the effect of iron in aluminum-silicon casting alloys is abundant, and demonstrates the importance of the nature of the intermetallics on the mechanical properties of the aluminum.

As an example, Bischofberger et al [19] studied the high cycle fatigue behaviour of cast Al-Si alloys (type GK-AlSi12CuMgNi) as a function of iron content. Figure 2.6 shows the influence of iron content on the mean fatigue strength at room temperature. A significant reduction in fatigue strength was found at the high iron level (1.5 wt%). They [19] also plotted (fig. 2.7) the fraction failure at different origins, for which identification of where the crack had started was accomplished by means of scanning electron fractography.

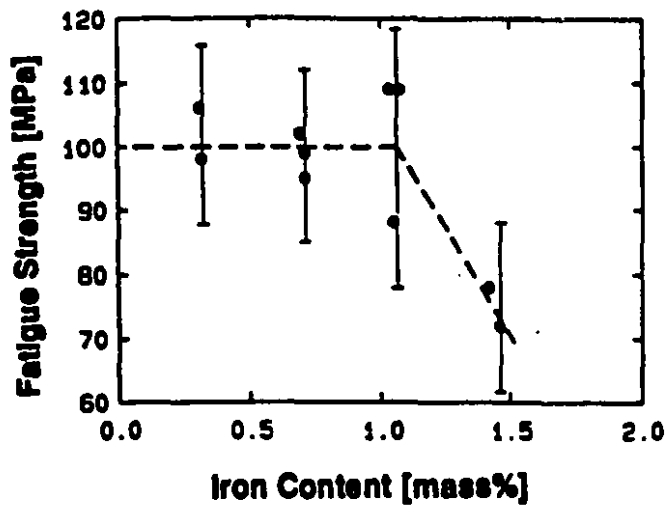

Figure 2.6 Fatigue strength versus iron content at room temperature [19]

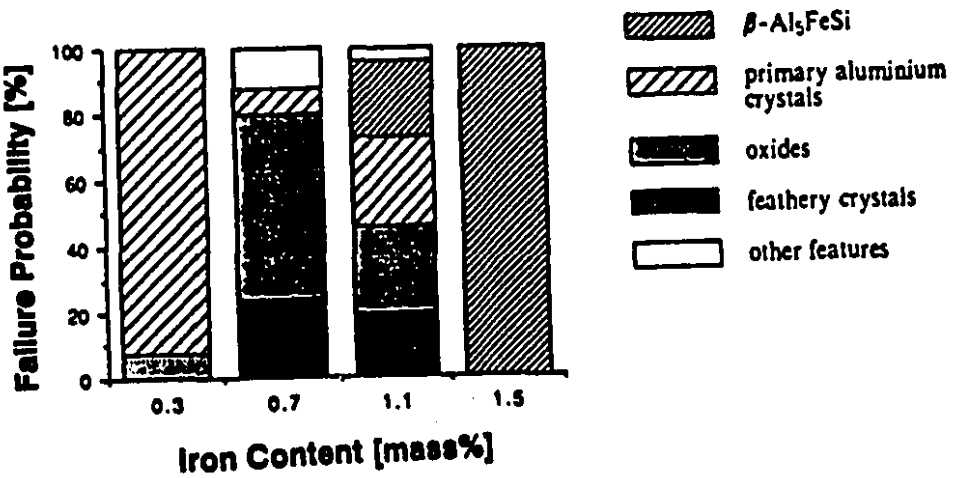

Figure 2.7 Fraction of failure at different origins [19]

2.4 STRONTIUM MODIFICATION

2.4.1 Strontium Modification in Al-Si Casting Alloys

The major use of strontium is as an additive to aluminum-silicon casting alloys. Strontium is a surface active element used to modify the eutectic silicon plates. A small addition of strontium (<0.02 weight percent) has been shown to alter the morphology from acicular plates to fine fibres. This modification results in improved mechanical properties, ductility and impact resistance of the castings [20,21,22]. The ability of strontium to modify the structure of the silicon phase raises the possibility that it may also be capable of changing the morphology of some intermetallic phases commonly found in wrought aluminum alloys.

2.4.2 Strontium Modification in 6000 Series Wrought Aluminum Alloys

The major alloying elements in the 6000 series extrusion alloys are silicon and magnesium in the approximately correct proportions to form magnesium silicide. Some of the silicon however, forms ternary Al-Fe-Si intermetallics with the iron impurities. The two predominant Al-Fe-Si intermetallic compounds present in these alloys are Al_8Fe_2Si (α-AlFeSi) and Al_5FeSi (β-AlFeSi). It has been found that a strontium addition of approximately 0.015 weight percent alters the morphology of Al-Fe-Si intermetallic phases found in alloys 6201 and 6063 from acicular (β-AlFeSi) to Chinese Script (α-AlFeSi) [23]. It is known that acicular β-AlFeSi in 6000 series alloys results in cracking during hot deformation processes, such as extrusion. Therefore, formation of the Chinese Script morphology (α-AlFeSi) is desirable as it benefits the extrusion properties of these alloys. As an example, acicular β-AlFeSi particles in alloy 6061 result in pick-up formation during the extrusion process due to the brittleness and abrasive nature of this phase [23]. The Chinese Script morphology (α-AlFeSi) is more compact and improves the ductility and extrudability of the alloy thus yielding improved properties and superior surface finish of the final product. Other transition elements such as manganese, chromium and cobalt are often added to the 6000 series alloys to promote the formation of Chinese Script intermetallic particles.

2.5 OBJECTIVES OF THE PRESENT WORK

Wrought aluminum alloys contain a wide variety of complex intermetallic phases which form during ingot solidification. The mechanical properties and workability of

these alloys depend largely on the nature of these intermetallic phases. The basic premise behind this study is that strontium is a surface active element capable of modifying the morphology of crystallographic phases such as those found in wrought aluminum alloys. Modification of these Al-Fe-Si intermetallics by strontium has shown potential to yield easier fabrication and improved properties in the end products of 6000 series alloys. The 1000 series wrought aluminum alloys, which are mainly rolling alloys, contain the same Al-Fe-Si intermetallic phases as the 6000 series. Modification of these phases could possibly increase the formability of these alloys. The present work assesses the modifying effect of strontium on intermetallic phases found in synthetic 1000 series alloys, and its subsequent influence on formability.

The study is divided into two parts; the first part includes the microstructural examination and quantification while the second part deals mainly with the mechanical properties. The research objectives are as follows:

(1) To determine the conditions under which α-AlFeSi and β-AlFeSi form in 1000 series wrought aluminum alloys upon solidification. The parameters investigated include the impurity level (i.e. Fe+Si total), the ratio of iron to silicon (Fe/Si), the cooling rate and the addition of strontium to the melt.

(2) To determine how the morphology of the Al-Fe-Si intermetallic phases affect the mechanical properties, in particular the formability, of the worked product.

CHAPTER
3

EXPERIMENTAL METHODS

3.1 GENERAL APPROACH

The first step in the experimental approach was to produce synthetic alloys with chemical composition ranges representing the 1000 series wrought aluminum alloys, with and without strontium. The various target parameters are summarized in table 3.1 below.

Table 3.1 Summary of target parameters

Parameter	Target Values
(Fe + Si) total	0.75, 1.0 and 1.5 wt%
Fe/Si	0.5, 1.0, 1.5 and 2.0
Strontium Addition	0, 0.02 and 0.06 wt%
Cooling Rate	1,2 and 7 °C/s

The total impurity level (Fe + Si) averages at about 0.75 weight percent and can be as high as 1 weight percent in the 1000 series. The average and maximum limits were chosen as target parameters along with a higher value which is 50% greater than the maximum limit (i.e. 1.5 wt%). This was done to test the alloy behaviour at an (Fe+Si) total which far exceeds the accepted maximum. The other specified parameter is the ratio of the iron to silicon (i.e. Fe/Si) which generally varies from 0.5 to 2.0 in

the 1000 series. These alloys are usually cast by the Direct Chill (DC) casting method and are mainly rolling alloys. Three molds were fabricated to provide varying cooling rates to simulate typical local cooling rates encountered in DC casting (1-10 °C/s). Samples were cast without strontium and at two levels of strontium additions. An addition of 0.02 weight percent was a guideline value taken from work on the 6000 series [23], and a higher value of strontium (i.e. 0.06 percent) was also chosen.

A section of each casting was rolled and annealed to produce a wrought product. The as-cast and rolled microstructures were analyzed and quantified using Image Analysis techniques. Mechanical testing which consisted of tensile testing and formability testing (Erichsen deformation tests) was performed on the rolled samples.

3.2 FABRICATION OF THE MOLDS

Three molds, two graphite and one copper, were fabricated to produce 1.5X10.6X15 cm aluminum castings. A schematic of the type of molds produced is shown in figure 3.1 and the dimensions are tabulated in table 3.2.

Table 3.2 Dimensions of molds (see fig 3.1)

Mold Type	Cooling Rate (°C/s)	X (mm)	Y (mm)
Small Graphite	1	33	15
Large Graphite	2	74	58
Copper	7	35	18

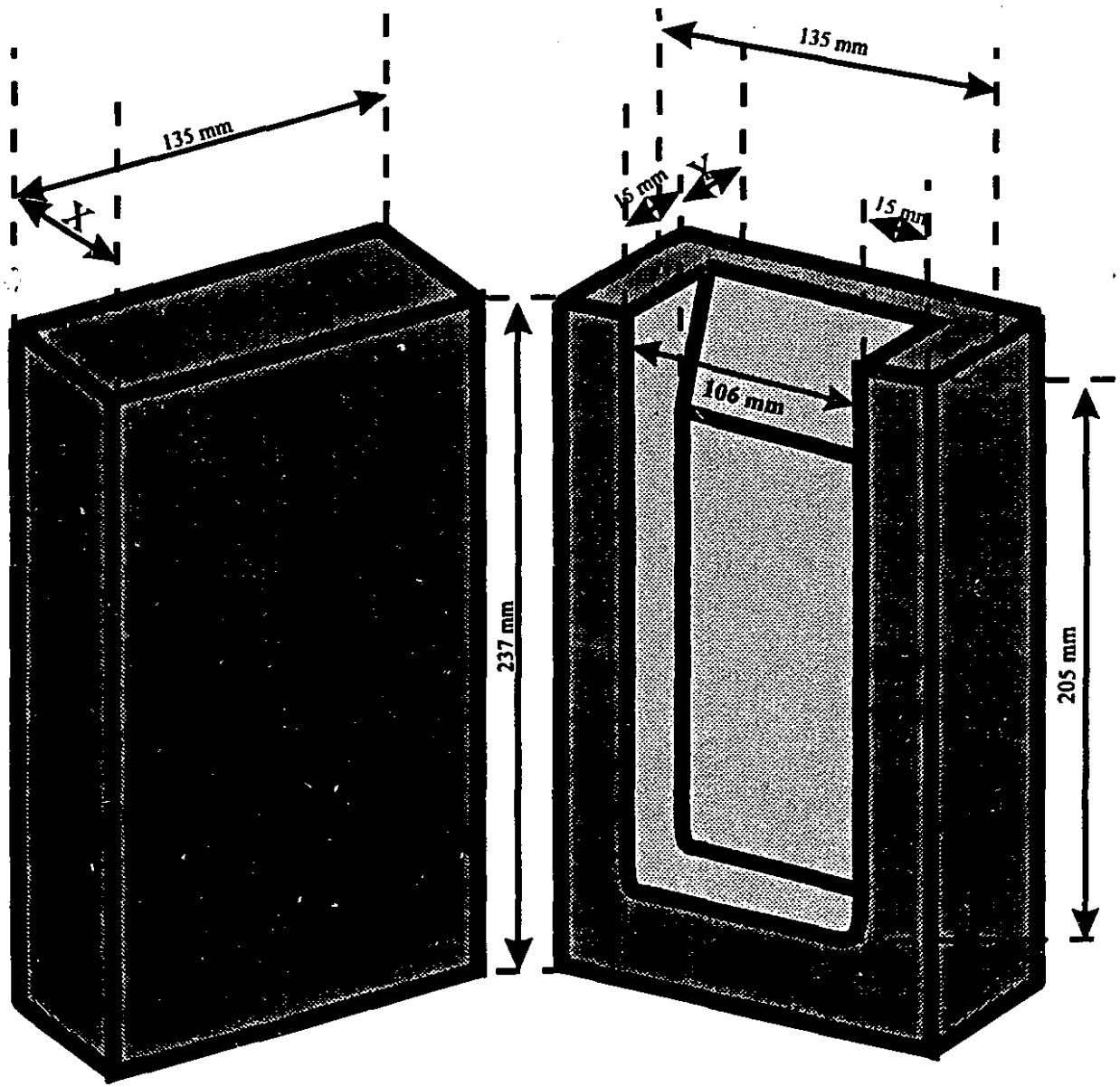

Figure 3.1 Schematic of casting mold

In order to determine the cooling rate during solidification of the samples, the secondary dendrite arm spacing (DAS) was measured and the rate was calculated using the following empirical relation [14]:

$$V = 3.57 \times 10^4 (DAS)^{-2.56}$$

where V = cooling rate (°C/sec)
DAS = dendrite arm spacing in microns

The dendrite arm spacing was calculated from lines drawn on optical micrographs as shown in figure 3.2. The calculation was done as follows:

$$\text{DAS (in microns)} = \frac{\text{length of line (mm)}}{\text{number of intercepts}} \times \frac{1000}{\text{Magnification}}$$

Figure 3.2 Optical micrograph showing aluminum dendrites

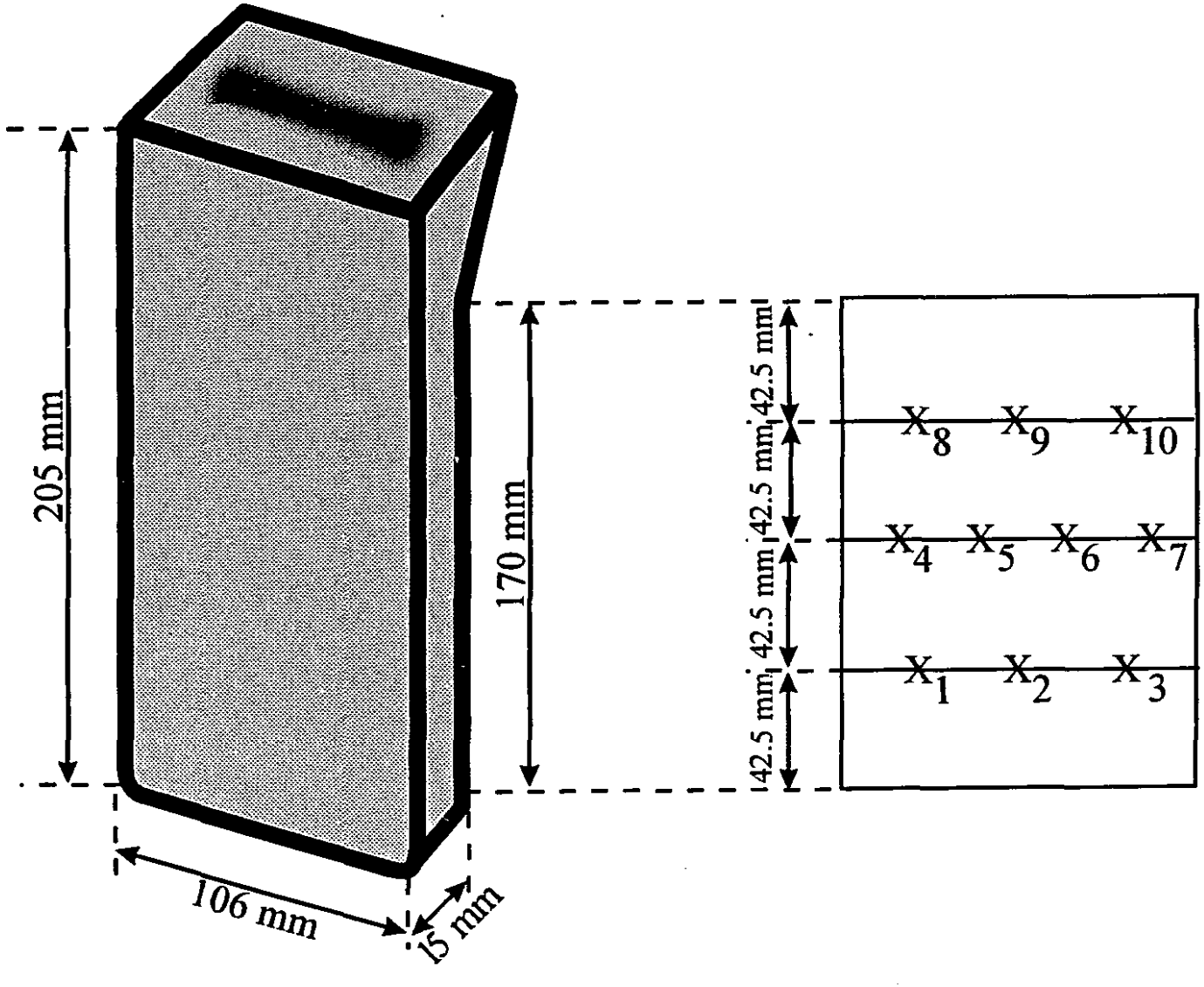

Figure 3.3 Schematic of casting showing sections analyzed

Two castings from each mold were analyzed at 10 different sections (see fig. 3.3) to determine the average cooling rate for the mold. The results are listed in table 3.3 .

Table 3.3 Cooling Rate Results (avg. of 20 sections)

Mold Type	DAS (microns)	Cooling Rate (°C/s)
Small graphite	60.7 ± 1.6	1.0 ± 0.1
Large graphite	46.7 ± 1.0	1.9 ± 0.1
Copper	27.8 ± 0.7	7.2 ± 0.4

3.3 CASTING PROCEDURE

Approximately 12 kilograms of pure aluminum (see table 3.4) were melted in an induction furnace, and the melt was heated to 750°C. The proper amounts of iron (added as 25Fe/75Al master alloy, table 3.4) and pure silicon were then added to the melt. The additions were allowed to dissolve for 15 minutes and then a sample was cast in each mold along with a sample for spectrochemical analysis. The recovery of iron and silicon was assumed to be 100 percent since these elements have very low vapour pressures. The melt was kept at temperatures of 700-710°C while the molds cooled back to room temperature (approx. 45 minutes). The appropriate amount of strontium (added as 10Sr/90Al master alloy, table 3.4) was then added to achieve a melt concentration of 0.02 weight percent strontium. This addition was allowed to dissolve for 5 minutes and

then samples were cast in the same manner as above. The recovery of strontium was assumed to be 100 percent for the first addition since it remained in the melt only 5 minutes prior to casting. Similarly, alloys containing 0.06 weight percent strontium were produced. However, during the 45 minutes between the two strontium additions (while the molds cooled back to room temperature), it was determined by chemical analysis that approximately 50 percent of the strontium had faded. Therefore, only 0.01 weight percent strontium was left in the melt prior to the second addition, requiring an addition of 0.05 weight percent strontium to produce the desired strontium level of 0.06 weight percent.

Table 3.4 Chemical composition of starting materials (wt%)

Element	Aluminum	Al-Fe Alloy	Al-Sr Alloy
Al	99.9	-	-
Si	0.03	0.05	0.05
Fe	0.05	24.7	0.13
Cu	<0.01	-	-
Mn	<0.01	0.15	-
Zn	0.01	0.01	0.02
V	<0.01	0.01	0.01
Ga	0.01	0.01	0.02
Ni	0.009	0.01	-
Sr	-	-	10.2
V	-	-	0.01
Ti	-	-	0.05
Ca	-	-	0.01
Ba	-	-	0.02

A total of 108 castings was produced for which the spectrochemical analysis results are listed in tables 3.5, 3.6 and 3.7.

Table 3.5 Chemical composition of synthetic alloys (Fe+Si= 1wt%)

Sample #	wt%Fe	wt%Si	wt%Sr	Cooling Rate (°C/s)
1	0.35	0.67	0	1
2	0.35	0.67	0	2
3	0.35	0.67	0	7
11	0.35	0.69	0.02	1
12	0.35	0.69	0.02	2
13	0.35	0.69	0.02	7
21	0.34	0.70	0.05	1
22	0.34	0.70	0.05	2
23	0.34	0.70	0.05	7
31	0.49	0.52	0	1
32	0.49	0.52	0	2
33	0.49	0.52	0	7
41	0.48	0.49	0.02	1
42	0.48	0.49	0.02	2
43	0.48	0.49	0.02	7
51	0.48	0.52	0.05	1
52	0.48	0.52	0.05	2
53	0.48	0.52	0.05	7
61	0.65	0.46	0	1
62	0.65	0.46	0	2
63	0.65	0.46	0	7
71	0.63	0.45	0.02	1
72	0.63	0.45	0.02	2
73	0.63	0.45	0.02	7
81	0.63	0.45	0.05	1
82	0.63	0.45	0.05	2
83	0.63	0.45	0.05	7
91	0.66	0.34	0	1
92	0.66	0.34	0	2
93	0.66	0.34	0	7
101	0.66	0.36	0.02	1
102	0.66	0.36	0.02	2
103	0.66	0.36	0.02	7
111	0.66	0.36	0.05	1
112	0.66	0.36	0.05	2
113	0.66	0.36	0.05	7

Table 3.6 Chemical composition of synthetic alloys (Fe+Si= 0.75wt%)

Sample #	wt%Fe	wt%Si	wt%Sr	Cooling Rate (°C/s)
121	0.29	0.56	0	1
122	0.29	0.56	0	2
123	0.29	0.56	0	7
131	0.29	0.55	0.02	1
132	0.29	0.55	0.02	2
133	0.29	0.55	0.02	7
141	0.30	0.54	0.05	1
142	0.30	0.54	0.05	2
143	0.30	0.54	0.05	7
151	0.37	0.38	0	1
152	0.37	0.38	0	2
153	0.37	0.38	0	7
161	0.38	0.40	0.02	1
162	0.38	0.40	0.02	2
163	0.38	0.40	0.02	7
171	0.38	0.42	0.05	1
172	0.38	0.42	0.05	2
173	0.38	0.42	0.05	7
181	0.48	0.32	0	1
182	0.48	0.32	0	2
183	0.48	0.32	0	7
191	0.49	0.30	0.02	1
192	0.49	0.30	0.02	2
193	0.49	0.30	0.02	7
201	0.50	0.32	0.05	1
202	0.50	0.32	0.05	2
203	0.50	0.32	0.05	7
241	0.49	0.26	0	1
242	0.49	0.26	0	2
243	0.49	0.26	0	7
251	0.50	0.28	0.02	1
252	0.50	0.28	0.02	2
253	0.50	0.28	0.02	7
261	0.49	0.28	0.05	1
262	0.49	0.28	0.05	2
263	0.49	0.28	0.05	7

Table 3.7 Chemical composition of synthetic alloys (Fe+Si= 1.5wt%)

Sample #	wt%Fe	wt%Si	wt%Sr	Cooling Rate (°C/s)
271	0.48	1.0	0	1
272	0.48	1.0	0	2
273	0.48	1.0	0	7
281	0.50	1.0	0.02	1
282	0.50	1.0	0.02	2
283	0.50	1.0	0.02	7
291	0.48	1.0	0.05	1
292	0.48	1.0	0.05	2
293	0.48	1.0	0.05	7
301	0.76	0.73	0	1
302	0.76	0.73	0	2
303	0.76	0.73	0	7
311	0.76	0.73	0.02	1
312	0.76	0.73	0.02	2
313	0.76	0.73	0.02	7
321	0.76	0.75	0.05	1
322	0.76	0.75	0.05	2
323	0.76	0.75	0.05	7
331	0.96	0.62	0	1
332	0.96	0.62	0	2
333	0.96	0.62	0	7
341	0.96	0.62	0.02	1
342	0.96	0.62	0.02	2
343	0.96	0.62	0.02	7
351	0.96	0.64	0.05	1
352	0.96	0.64	0.05	2
353	0.96	0.64	0.05	7
361	0.96	0.48	0	1
362	0.96	0.48	0	2
363	0.96	0.48	0	7
371	0.96	0.51	0.02	1
372	0.96	0.51	0.02	2
373	0.96	0.51	0.02	7
381	0.96	0.53	0.05	1
382	0.96	0.53	0.05	2
383	0.96	0.53	0.05	7

3.4 ROLLING AND ANNEALING

A piece from each casting (1.5 X 6 X 10.6 cm) was rolled down to 1mm thickness to provide a wrought product for microstructural analysis and mechanical testing. A few samples were rolled at McGill, however it was determined that the surface quality was poor and would definitely affect the Erichsen measures of formability. Therefore, the samples were rolled at the Alcan Research & Development Centre in Kingston. The samples were heated to 500°C for approximately 20 minutes and were then hot rolled down to 1mm through 18 passes at 0.76 mm reduction each pass (0.030"/pass). Since the samples were relatively small, it is possible that enough heat loss occurred during rolling to allow the material to be work hardened near the end of the rolling process. To ensure that no work hardening remained after rolling, the sheet samples were annealed after rolling in a furnace at 500°C for 2 hours. One half of each sheet was used to cut tensile samples at McGill while the remaining half of the sheet underwent Erichsen ball punch deformation testing at Alcan.

3.5 MICROSTRUCTURAL QUANTIFICATION

Microstructural quantification was performed on each casting to determine the relative amounts of each intermetallic phase in the as-cast structures. Selected rolled samples were also microstructurally quantified to determine particle sizes and distributions in the wrought structure. Both the as-cast and wrought samples were prepared in the same manner.

3.5.1 Sample Preparation

A small piece was cut from the centre (see fig 3.3, area between X_5 and X_6) of each casting and the edges were smoothed out with a coarse 60 grit silicon carbide paper. The pieces cut from the rolled samples were only 1mm thick and were cold mounted with epoxy prior to grinding. Each sample then underwent the following wet grinding: 240, 400 and 600 grit silicon carbide papers. The samples were placed in an ultrasonic bath to remove coarse debris from the grinding process. The samples were then polished with 5 micron and then 0.3 micron solution of alumina (Al_2O_3) in suspension in water. A final polishing was performed with a colloidal silica solution. A solution of 0.5 volume percent hydrofluoric acid (HF) was used to etch the samples for approximately 10 seconds. The samples were rinsed in methanol and dried with a hair dryer.

3.5.2 Electron Probe Microanalysis

Chemical analysis of the various particles in the microstructure was performed on six selected samples using the Joel JXA-8900L WD/ED combined microanalyzer on a scanning electron microscope (SEM). The samples were prepared as explained above and were carbon coated to ensure conductivity in the SEM.

3.5.3 Optical Microscopy

Optical microscopy was performed using a Leco image analyzer interfaced with an optical microscope through the 2005 image analysis program. This system distinguishes different phases based on 256 grey levels. Five selected samples were microstructurally quantified on 50 fields at a magnification of 500X. Figure 3.4 shows the results for sample #301 which was solidified at the slowest cooling rate (1 °C/s) and contained the highest level of impurities (1.5 wt%). Similar graphs were plotted for other samples with lower impurity levels and higher cooling rates. It was experimentally determined that observation of 25 fields at a magnification of 500X was sufficient to obtain a representative area of the sample.

The area percent of each phase was measured in the as-cast condition based on the morphology differences and was used in the determination of the volume fraction of the intermetallic phases. It was difficult to obtain a difference in grey levels for the α-AlFeSi and β-AlFeSi phases, probably due to the small differences in their chemical compositions. Therefore, the quantification of the intermetallic phases was accomplished through user interaction to identify to the system the various phases based on morphological differences.

In the rolled samples, the intermetallics were broken into small particles (figure 3.5) for which it was impossible to identify the phases through optical microscopy. These particles were sized and quantified to produce particle size distributions for selected samples.

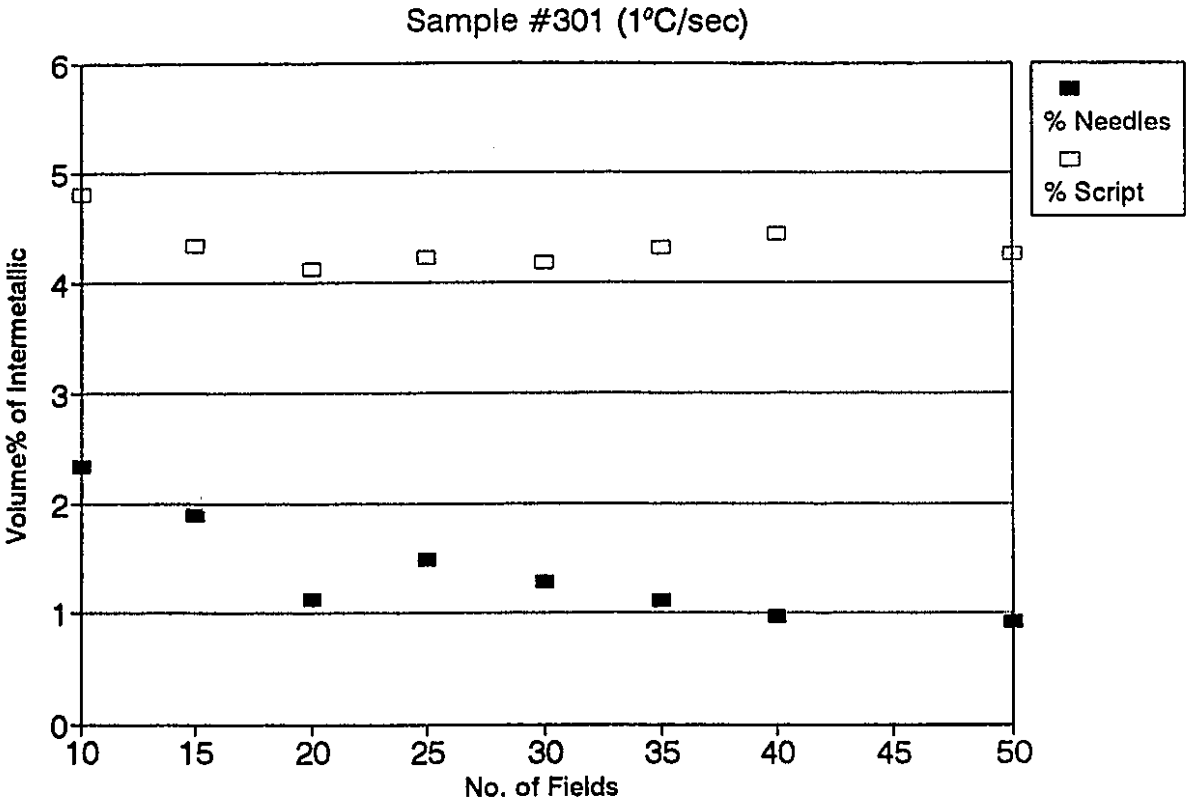

Figure 3.4 Quantitative metallography results

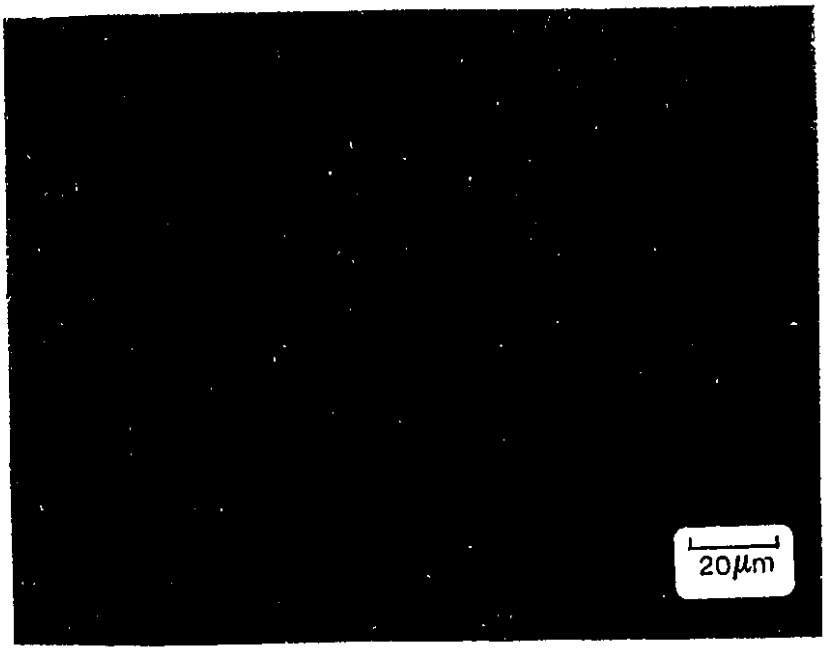

Figure 3.5 Typical Microstructure of a rolled sample

3.6 MECHANICAL TESTING

3.6.1 Tensile Testing

Tensile bars from each 1mm thick sheet were cut at McGill with a 2 cm gage length. One half of the samples was pulled at McGill using the Instron tensile machine. Four tensile bars were pulled for each sample at a rate of 5mm/min. A strain gage was used to record the yield point and a 2 cm gage length was drawn on the sample to determine the percent elongation. The remaining samples were pulled at the Alcan Research & Development Centre under the same conditions as above.

3.6.2 Formability Testing

Each rolled sheet was tested using the Erichsen ball punch deformation method to measure formability. Six ball punch deformation tests were performed on each 1mm sheet specimen. This is a standard test method used to evaluate and compare the formability of metallic sheet materials. Figure 3.6 shows the ball punch deformation test tooling.

The constrained sheet metal specimen is bulged at a specified rate until the load drops or until either necking or fracture occurs. The experiments were carried out with a constant hold-down force of 1000 kilograms. The height of the cup formed, as shown in figure 3.7, is the measure of formability. The predominant mode of deformation is biaxial stretching and therefore the results from this test are most often used to rate or compare materials that are to be formed mainly by stretching [25].

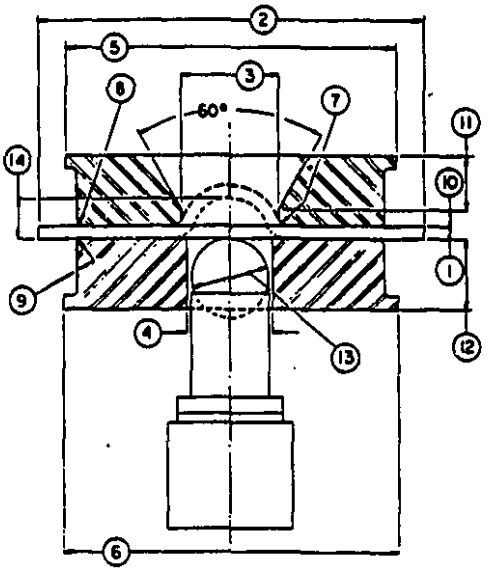

Key		Dimensions	
		in.	mm
①	Thickness of test piece	full thickness	full thickness
②	Width of test piece (minimum)	3.5	90
③	Bore diameter of top die	see 6.3	see 6.3
④	Bore diameter of bottom die	1 ± 0.004	25.4 ± 0.1
⑤	External diameter of top die (approximate)	3.5	90
⑥	External diameter of bottom die (approximate)	3.5	90
⑦	Corner radius of interior of top die	0.032 ± 0.002	0.81 ± 0.05
⑧	Corner radius of exterior of top die	0.032	0.8
⑨	Corner radius of exterior of bottom die	0.032	0.8
⑩	Depth of bore of top die	0.197 ± 0.010	5 ± 0.2
⑪	Thickness of top die (minimum)	0.78	20
⑫	Thickness of bottom die (minimum)	0.78	20
⑬	Diameter of spherical end of penetrator[A]	0.875 ± 0.002	22.22 ± 0.04
⑭	Depth of cup	depth of cup	depth of cup

[A] "Olsen" Ball, 22.22 mm (⅞ in.); "Erichsen" Ball, 20 mm.

Figure 3.6 Ball punch deformation test tooling [25]

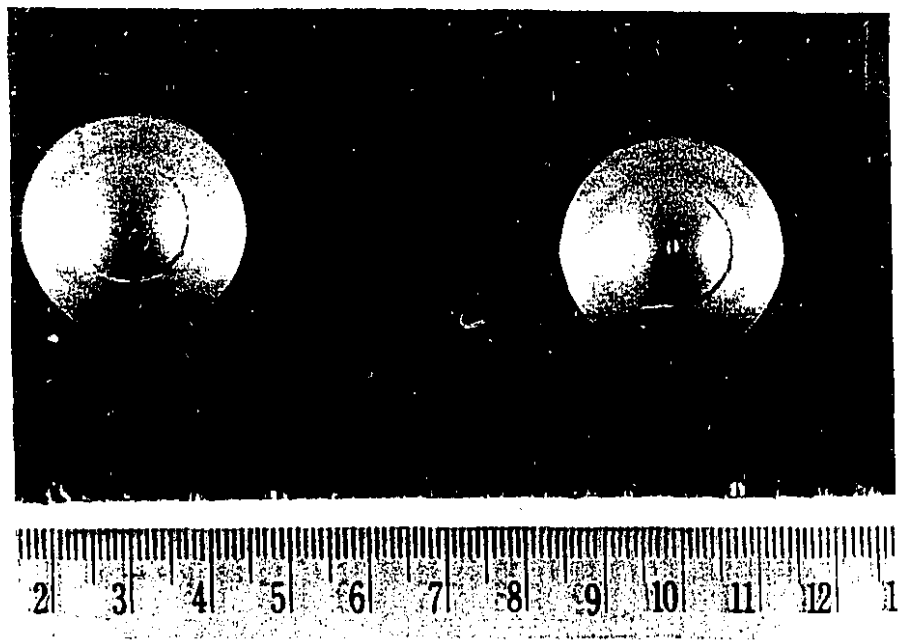

Figure 3.7 Cups formed in ball punch deformation testing

CHAPTER
4

RESULTS & DISCUSSION

This chapter is divided into two main sections. The first part deals with the microstructural examination and quantification of both the as-cast and rolled structures. The second part deals with the mechanical properties of the rolled product. It is generally believed that the appearance of intermetallic phases in the cast structure strongly influences the mechanical properties of the worked product. However, very little experimental work has been performed to prove this in the 1000 series wrought aluminum alloys. This study attempts to determine how the morphology and quantity of intermetallic phases in the as-cast structure influences the mechanical properties of the alloy.

4.1 PART I: QUANTITATIVE METALLOGRAPHY

4.1.1 As-cast Microstructures

The objective of the first part of this study was to quantify the intermetallic phases in the cast structure as a function of chemical composition and solidification rate. There were four parameters investigated: Fe/Si ratio, cooling rate, (Fe+Si) total and strontium level.

Optical microscopy of the as-cast structures revealed two main intermetallic morphologies in the inter-dendritic regions. These were assumed to be the ternary α-AlFeSi (Al_8Fe_2Si) which has a Chinese Script morphology (see figs 2.2 and 4.2) and the acicular β-AlFeSi (Al_5FeSi) (see figs 2.3 and 4.1). These are the two predominant ternary phases normally observed in these alloys as listed in table 2.3 in the literature review. This assumption was verified for selected samples using an electron probe microanalyzer (EPMA) on a scanning electron microscope. Since the particles were small (approx. 1 micron in thickness), aluminum from the surrounding dendrites interfered with the analysis and thus it was not possible to determine the exact stoichiometry of the phases. However, the atomic ratio of Fe/Si was sufficient to distinguish the different phases. The ternary α-AlFeSi (Al_8Fe_2Si) has an atomic ratio of Fe/Si of 2 while the acicular β-AlFeSi (Al_5FeSi) has a ratio of 1. The results from the electron probe microanalysis (EPMA) are given in table 4.1.

The atomic ratio of Fe/Si for the Chinese Script in the first five selected representative samples corresponds very well to the ideal ratio of 2. The ratio for the acicular β-AlFeSi was slightly lower than the ideal ratio of 1. This is probably due to interference from the dissolved silicon in the aluminum matrix. This effect was not seen with the Chinese Script morphology because an entire area of the Script network was analyzed whereas this was not possible with the thin individual β-particles. Figures 4.1 and 4.2 show secondary electron images of the β-AlFeSi and α-AlFeSi, respectively.

Table 4.1 EPMA Results

Sample		Atomic ratio Fe/Si (avg. 5 particles)	
Conditions	wt% ratio Fe/Si	Chinese Script morphology	Plate-like morphology
(Fe+Si)= 0.75 wt% Rate = 1°C/s	0.5 2.0	- 2.08 ± 0.05	0.88 ± 0.04 -
(Fe+Si)= 1.5 wt% Rate = 2 °C/s	0.5 1.0 1.5	- 1.97 ± 0.06 2.07 ± 0.05	0.90 ± 0.04 0.87 ± 0.05 -
exception* (Fe+Si)= 1.5 wt% Rate = 7 °C/s	2.0	2 types found: (1) 2.08 ± 0.06 and (2) no Si, 11 at%Fe	0.88 ± 0.06

*This sample was chosen because it showed exception to all tendencies.

The last sample in table 4.1 was analyzed because this was the only exception to every tendency observed in this study. As expected, a third intermetallic phase with the Chinese Script morphology was present in this sample. However, the Chinese Script of this phase was found to be slightly different than the representative morphology throughout this study. Figure 4.3 shows the secondary electron image of this phase which seems to be less of a continuous network in comparison to the ternary α-AlFeSi Chinese Script. This phase consisted only of iron (approx. 11 atom%) and aluminum, and is most likely binary Al_6Fe or Al_9Fe_2.

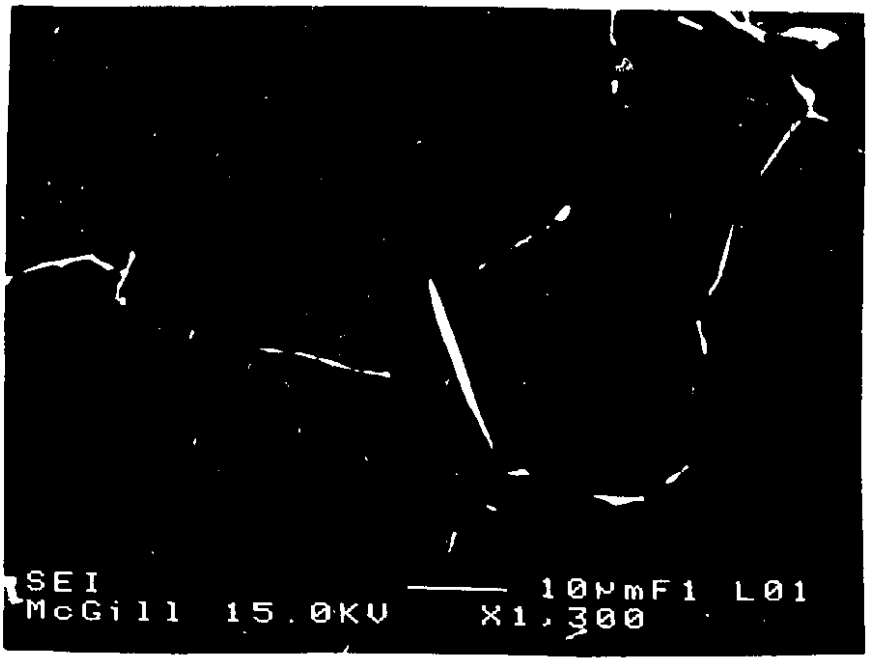

Figure 4.1 Secondary Electron Image of β-AlFeSi Particles

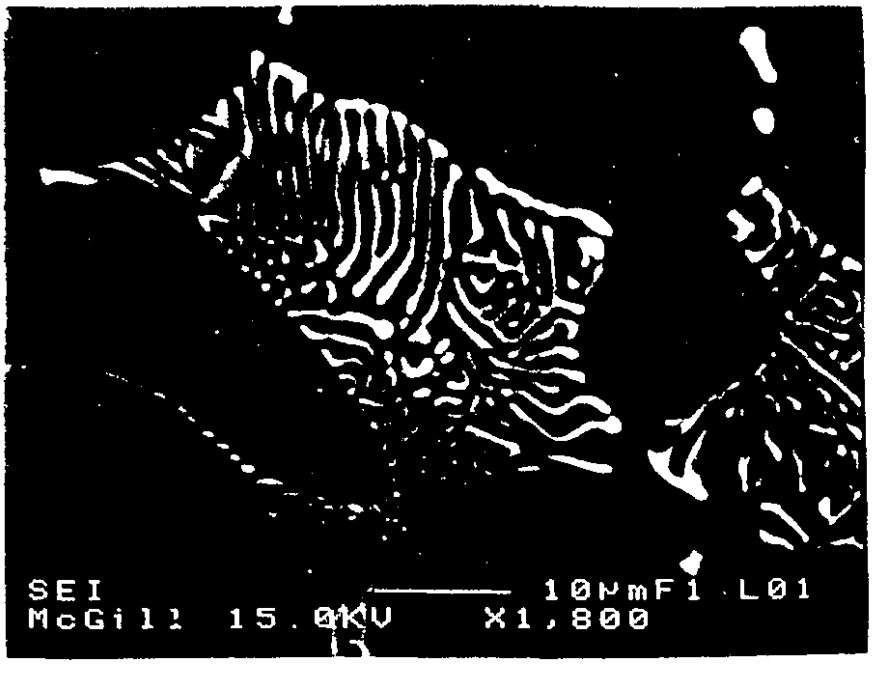

Figure 4.2 Secondary Electron of α-AlFeSi Chinese Script

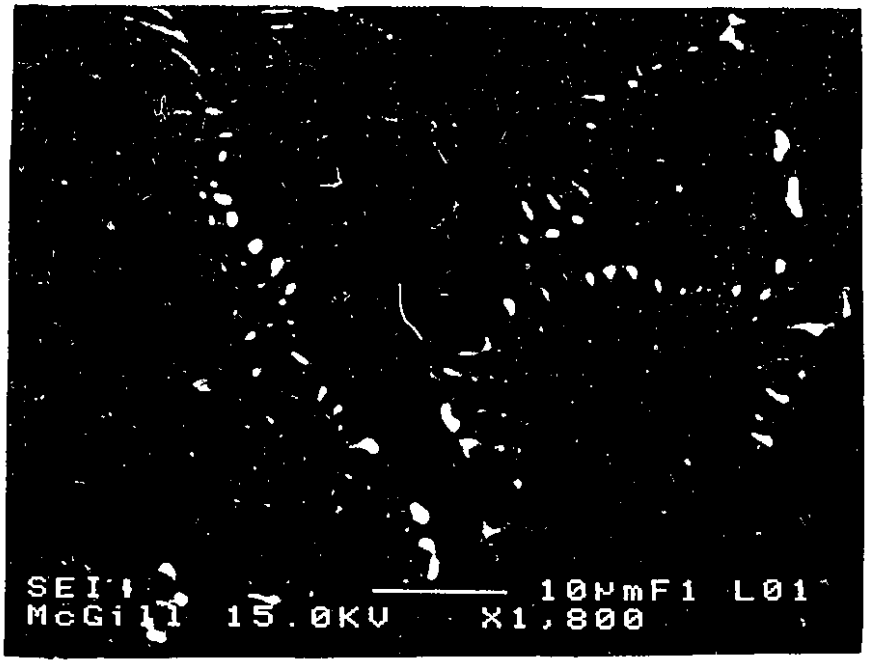

Figure 4.3 Secondary Image of Binary Al-Fe Chinese Script

Table 2.3 (in literature review) lists several binary phases that can form in these types of alloys. The binary Al_3Fe phase was not expected to form since the cooling rates were all above 1°C/s, however it is possible that small amounts of Al_3Fe needles were mistaken for β-AlFeSi particles in samples with lower cooling rates, however none was found with the EPMA. It is also possible that some Al_6Fe formed in samples with high iron contents. Since its morphology resembles that of the ternary α-Chinese Script, small amounts of Al_6Fe may have been counted as α-AlFeSi.

Quantitative metallography was performed to determine the total percentage of intermetallics in each sample as well as the proportion of intermetallics with the Chinese Script morphology (assumed to be predominantly the ternary α-Al_8Fe_2Si). The samples are grouped according to their total impurity level (Fe+Si) and the complete set of quantitative metallography results are given in Appendix A. The results for the samples without any strontium modification are presented in table 4.2 below.

Table 4.2 Relative %Chinese Script in intermetallics (no Sr modification)

Fe/Si	Rate (°C/s)	(Fe+Si) total		
		0.75 wt%	1.0 wt%	1.5 wt%
0.5	1	0	0	0
	2	0	0	0
	7	0	0	0
1.0	1	88.0	33.6	29.4
	2	100	58.3	61.2
	7	100	63.7	100
1.5	1	100	57.3	64.7
	2	100	100	100
	7	100	100	100
2.0	1	100	92.5	75.9
	2	100	100	100
	7	100	100	51.9

4.1.1.1 Effect of Fe/Si Ratio

The quantitative metallography results presented above indicate a strong tendency for the α-AlFeSi Chinese Script phase to form with increasing Fe/Si ratios. This trend corresponds well with the Al-Fe-Si phase diagram (figure 2.1). As the Fe/Si ratio decreases, formation of β-AlFeSi which is the more Si-rich phase is promoted. This effect is more pronounced at the two higher impurity levels (1 and 1.5 wt%). Figure 4.4 shows the increase in amount of Chinese Script in the intermetallic phase for a cooling rate of 1°C/s and impurity level of 1.0 weight percent (Fe+Si), without strontium modification.

This tendency is found for all three (Fe+Si) levels and cooling rates with the sole exception of the alloy having the highest impurity level (1.5 wt%), an Fe/Si ratio of 2

solidified at the fastest cooling rate (7°C/s). This sample was analyzed with the EPMA and a third intermetallic phase was discovered, as mentioned in the previous section. It was found that the excess iron in this sample formed a binary metastable Al-Fe compound (such as Al_6Fe, Al_9Fe_2 or Al_xFe), having a Chinese Script morphology similar to that of α-AlFeSi. The ternary β-AlFeSi phase was also found in this alloy, and this was not expected since none was found for the same conditions at lower (Fe+Si) levels. It is most likely that the binary Al-Fe phase formed first allowing the excess silicon in this sample to form the more Si-rich ternary β-phase.

Furthermore, in alloys containing higher amounts of silicon than iron (i.e. Fe/Si = 0.5), the microstructures consisted entirely of plate-like β-AlFeSi regardless of the impurity level and cooling rate. In some cases, by changing the Fe/Si ratio from 0.5 to 1.0, the intermetallic phase in the microstructure changed from 100 percent β-AlFeSi to 100 percent α-Chinese Script. The optical micrographs in figure 4.5 demonstrate the change in morphology of the Al-Fe-Si constituents by varying the Fe/Si ratio for a given (Fe+Si) total of 0.75 weight percent and cooling rate of 2 °C/s. Figure 4.5a shows the microstructure obtained at an Fe/Si ratio of 0.5 consisting entirely of plate-like β-AlFeSi particles. The microstructure for the same conditions with an Fe/Si ratio of 1.0 consisted only of α-AlFeSi (fig. 4.5b). Similar observations have been reported by others. For example, Turmezey [26] reported that in alloys with higher silicon contents (i.e. Fe/Si < 1), only the β-AlFeSi phase is formed as part of a eutectic, independent of the cooling rate.

Figure 4.4 Effect of Fe/Si Ratio
(Fe+Si) = 1.0 wt%, 1°C/s

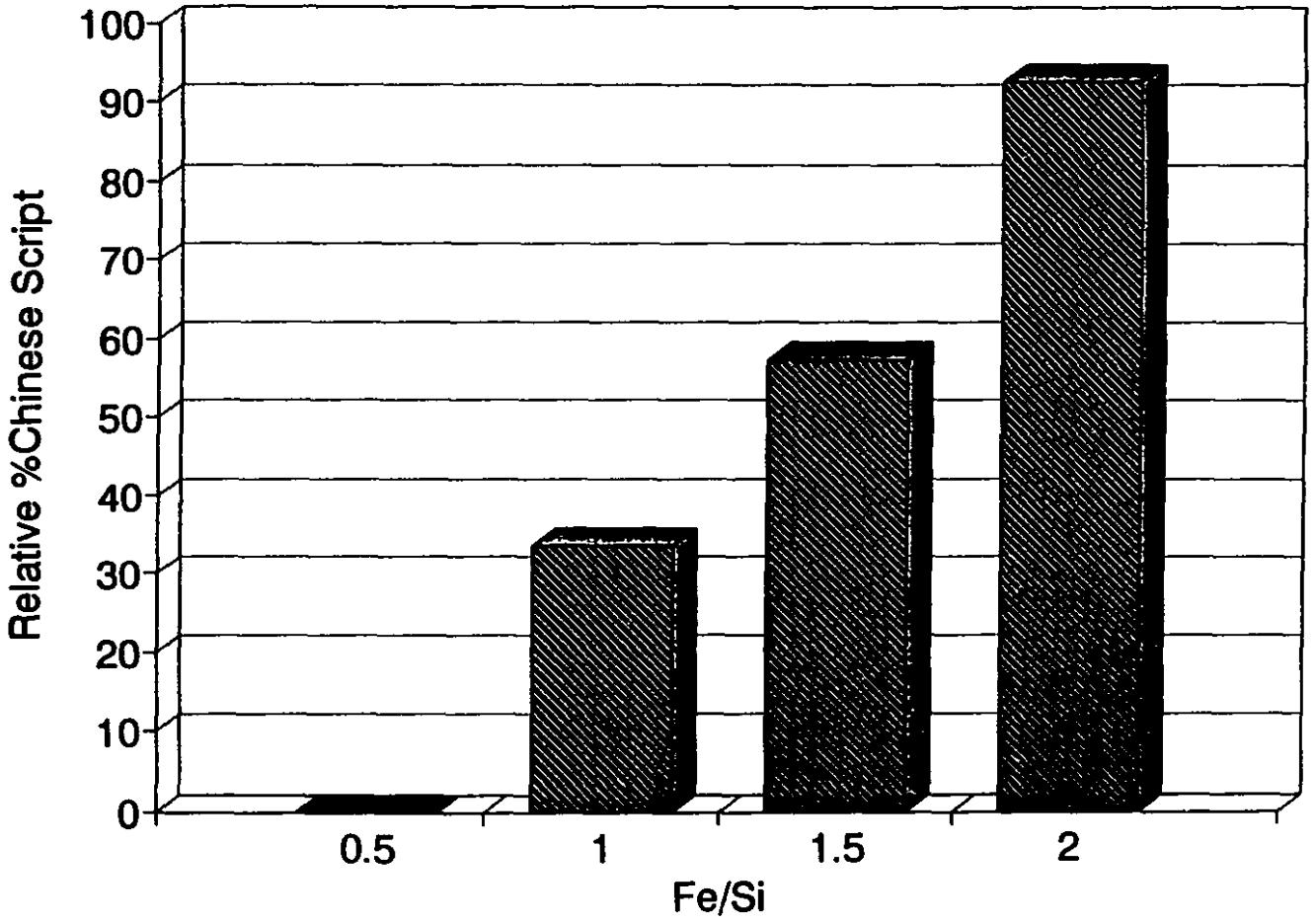

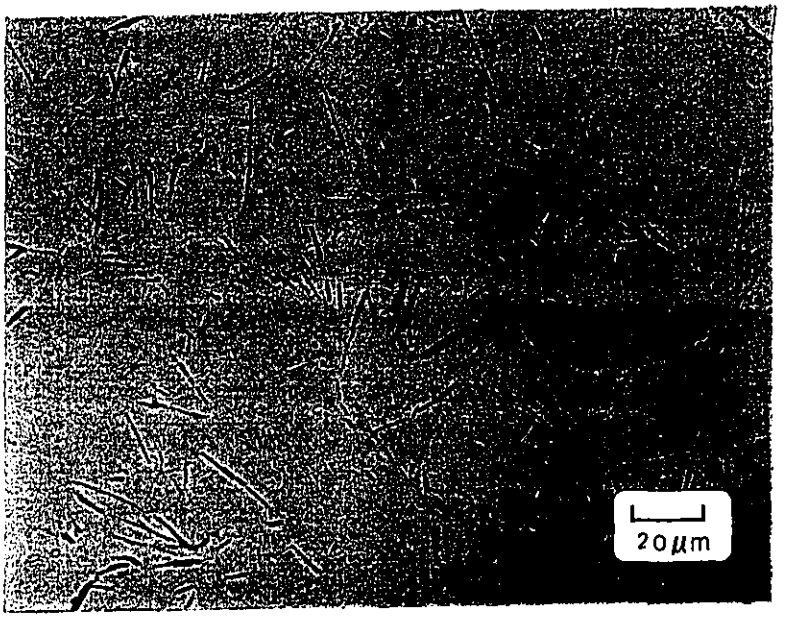

(a) Fe/Si = 0.5

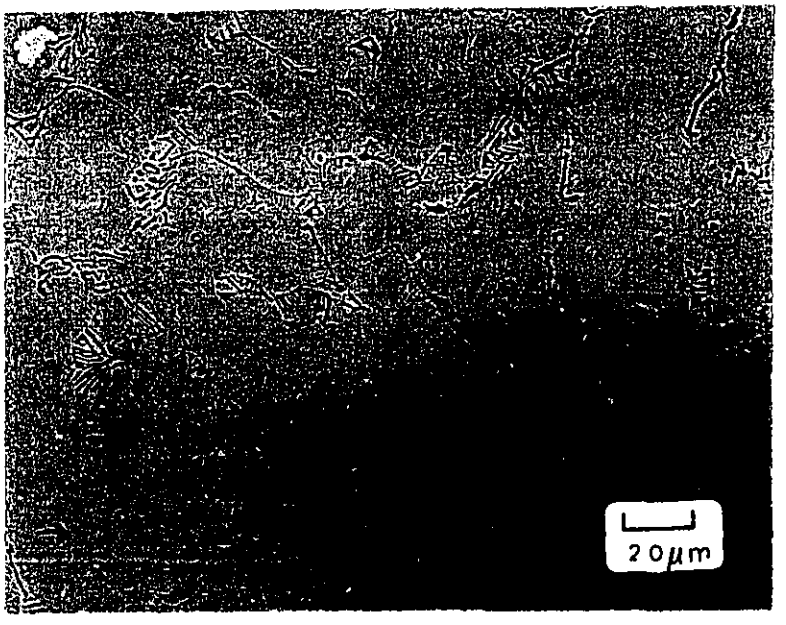

(b) Fe/Si = 1.0

Figure 4.5 Optical micrographs showing effect of Fe/Si ratio

4.1.1.2 Effect of Cooling Rate

As the cooling rate increases for a given Fe/Si ratio, there is a strong tendency for α-Chinese Script phase formation. Figure 4.6 presents the results for the three cooling rates at the different impurity levels and a constant Fe/Si ratio of 1.0. The tendency for more α-Chinese Script to form with increasing cooling rate is less pronounced for alloys with 0.75 percent (Fe+Si) and is more clearly shown in alloys containing 1 and 1.5 percent (Fe+Si). Again, the alloy with the highest impurity level (1.5 wt%), Fe/Si ratio of 2 and the fastest cooling rate is the sole exception to the observed trend. The tendency for more Chinese Script to form with increasing cooling rate has been observed by others. Skjerpe [27] reported that α-AlFeSi Chinese Script was the dominating phase in regions with high cooling rates (6-8 K/s). However, other scientists have reported conflicting results. Dons [8] observed a shift toward Si-richer particles (i.e. β-AlFeSi) with increased rate of cooling. Also, Langsrud's [3] model for the precipitation of AlFeSi-particles during solidification predicted a tendency for more Si-rich phases to form as the cooling rate increases. The "metastable" diagrams for different cooling rates suggested by Langsrud [3] are presented in figure 2.5 in the literature review.

As mentioned in the previous section, alloys containing higher amounts of silicon than iron (i.e. Fe/Si= 0.5) consisted entirely of plate-like β-AlFeSi particles regardless of the cooling rate. Therefore, the tendency for α-Chinese Script formation to increase with increasing cooling rate is only seen in alloys with higher amounts of iron than silicon (i.e. Fe/Si >= 1).

Figure 4.6 Effect of Cooling Rate
Fe/Si = 1.0

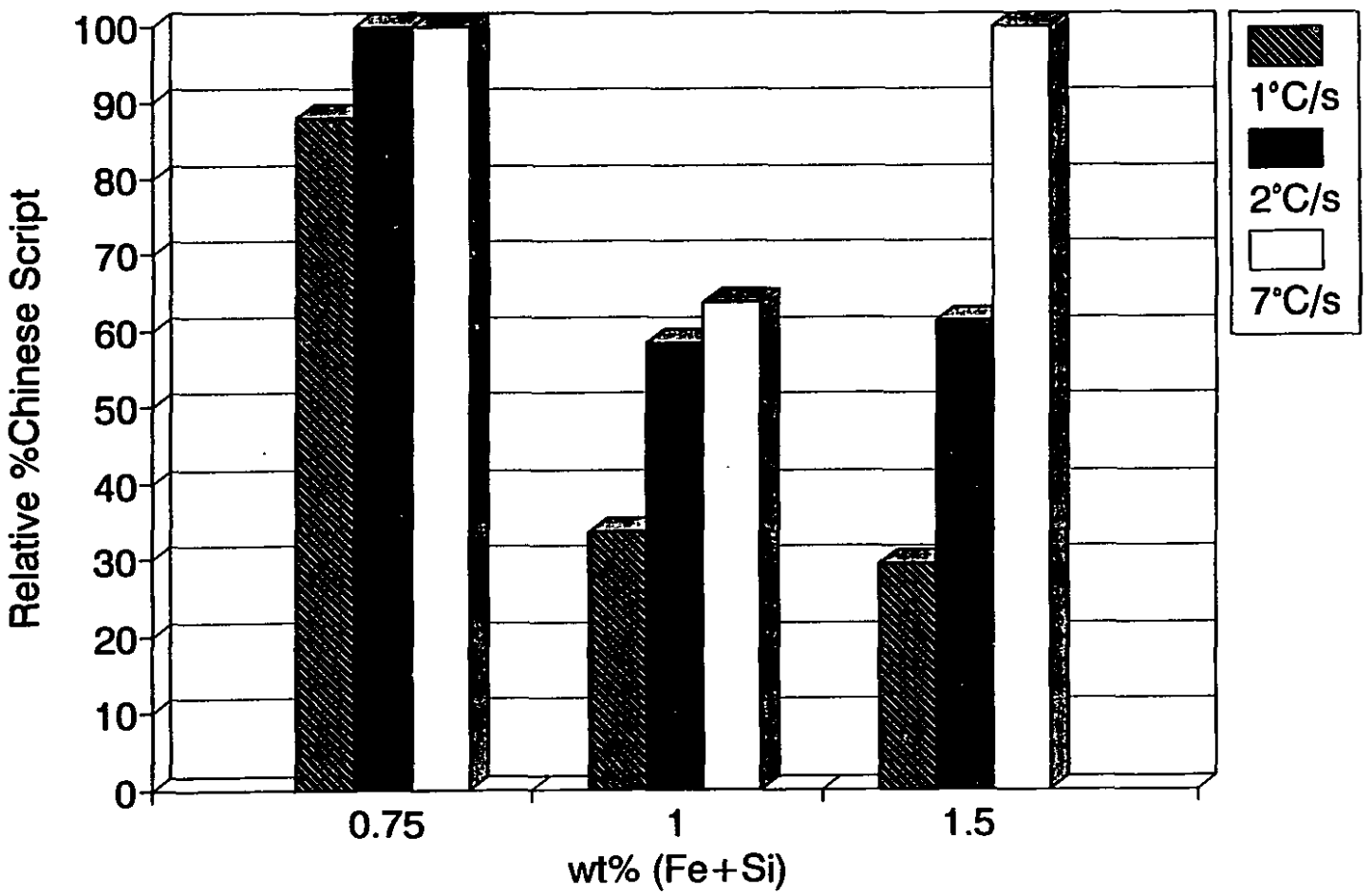

4.1.1.3 Effect of Impurity Level (Fe+Si)

There is a general tendency for the amount of Chinese Script in the microstructure to decrease with increasing amounts of impurities (Fe+Si). Figure 4.7 shows this tendency at a constant cooling rate of 1°C/s for the different Fe/Si ratios. As with the cooling rate, the impurity level tendency does not hold for alloys with low Fe/Si ratios (i.e. Fe/Si < 1). This general trend was also reported by Langsrud [3]. He concluded that for a given Fe/Si ratio, there is a tendency for more Si-rich particles (β-AlFeSi) to form as the alloying content increases.

The average volume percentage of intermetallics for the three levels of (Fe+Si) are listed in table 4.3 which shows that with increasing (Fe+Si) total, the total volume percent of intermetallics increases. These results are plotted in figure 4.8 where it is seen that the relationship is linear.

Table 4.3 Volume percent intermetallics at different (Fe+Si) totals

(Fe+Si) wt%	Volume % Intermetallics ($\alpha+\beta$)
0.75	1.9 ± 0.7
1.0	2.9 ± 0.8
1.5	5.2 ± 1.2

Figure 4.7 Effect of Impurity Level
Cooling Rate = 1.0°C/s

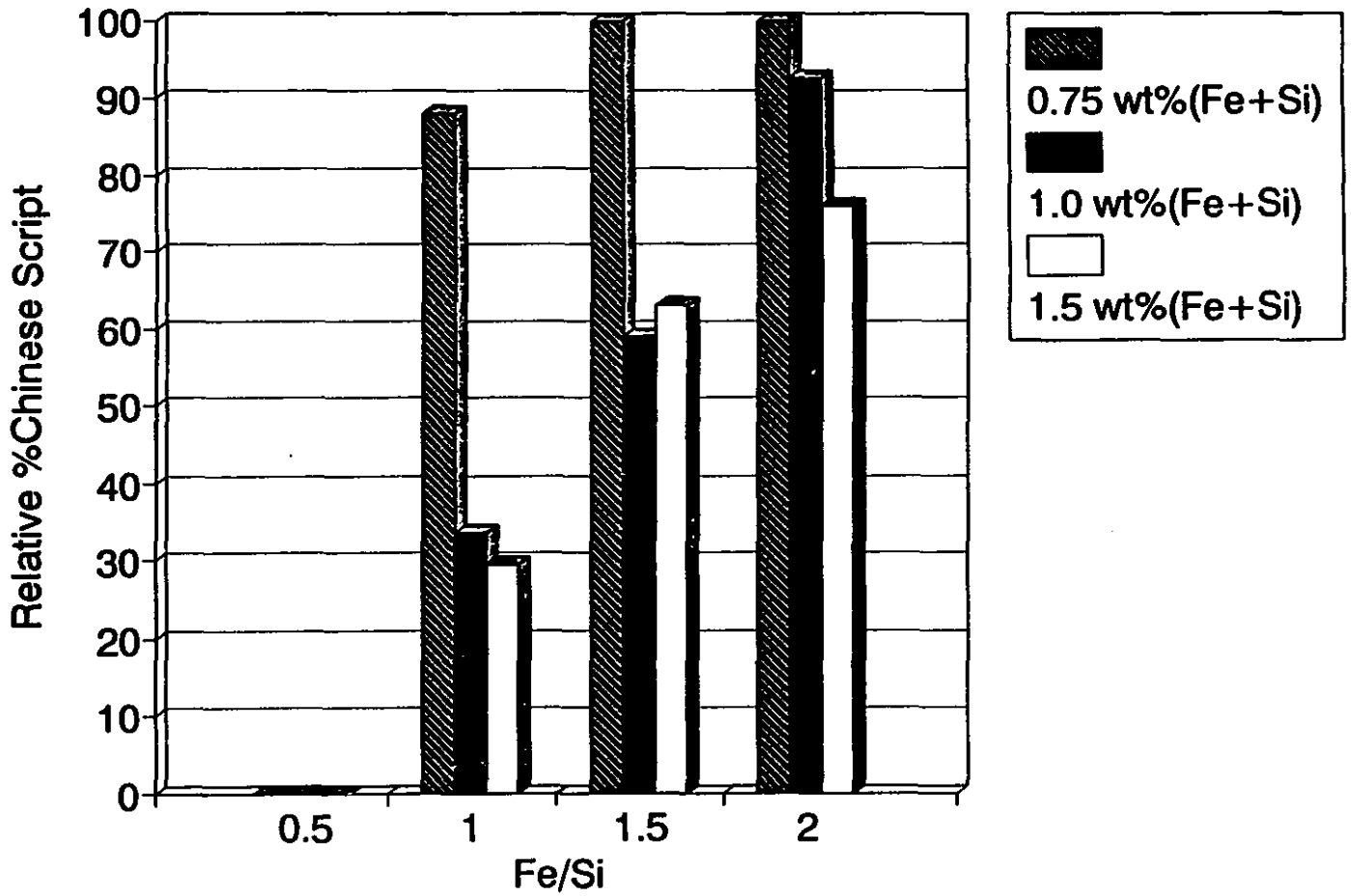

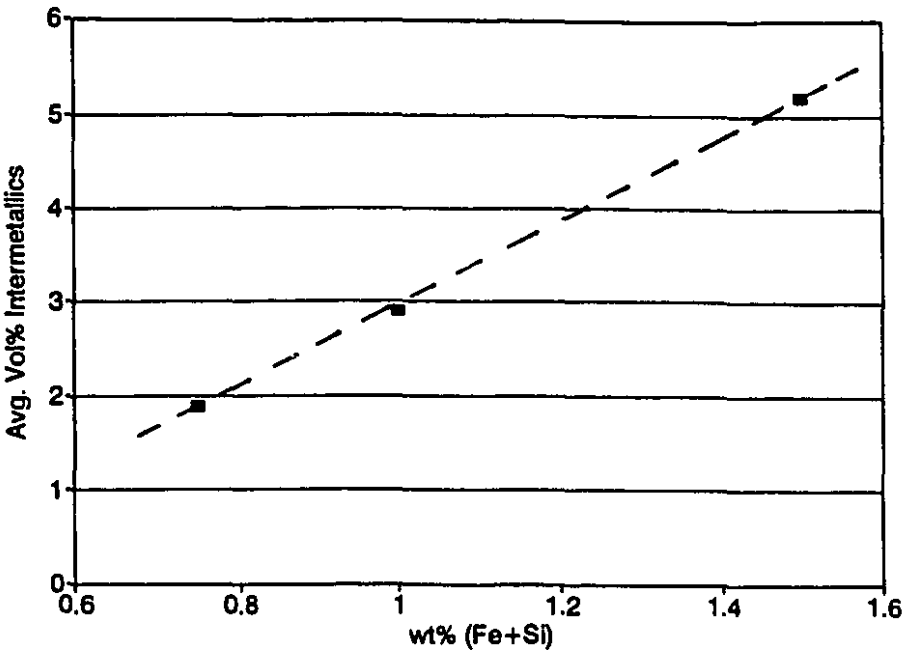

Figure 4.8 Volume percent intermetallics versus (Fe+Si) total

4.1.1.4 Effect of Strontium Addition

The amount of Chinese Script present in samples containing strontium additions is presented in table 4.4. The addition of strontium proved to promote the formation of α-AlFeSi Chinese Script. For alloys with Fe/Si ratio of 0.5, the strontium addition was very effective at the two lower (Fe+Si) totals (i.e. 0.75 and 1.0 wt%) and resulted in almost 100 percent of Chinese Script formation in alloys with 0.06 weight percent strontium. Figure 4.9 shows the effect of strontium addition for a constant Fe/Si ratio of 0.5 and cooling rate of 7 °C/s. Without any strontium, all three alloys contained no Chinese Script in the microstructure. For the alloys with (Fe+Si) totals of 0.75 and 1.0 percent, an addition of 0.02 percent strontium increased the relative percent Chinese Script in the microstructure to 53.0 and 23.7 respectively. However, the 0.02 percent strontium addition did not promote α-Chinese Script formation in the alloy with the highest (Fe+Si) total (i.e. 1.5 wt%). An addition of 0.06 percent to the two alloys with

Figure 4.9 Effect of Sr Addition
Fe/Si = 0.5, Cooling Rate = 7.0°C/s

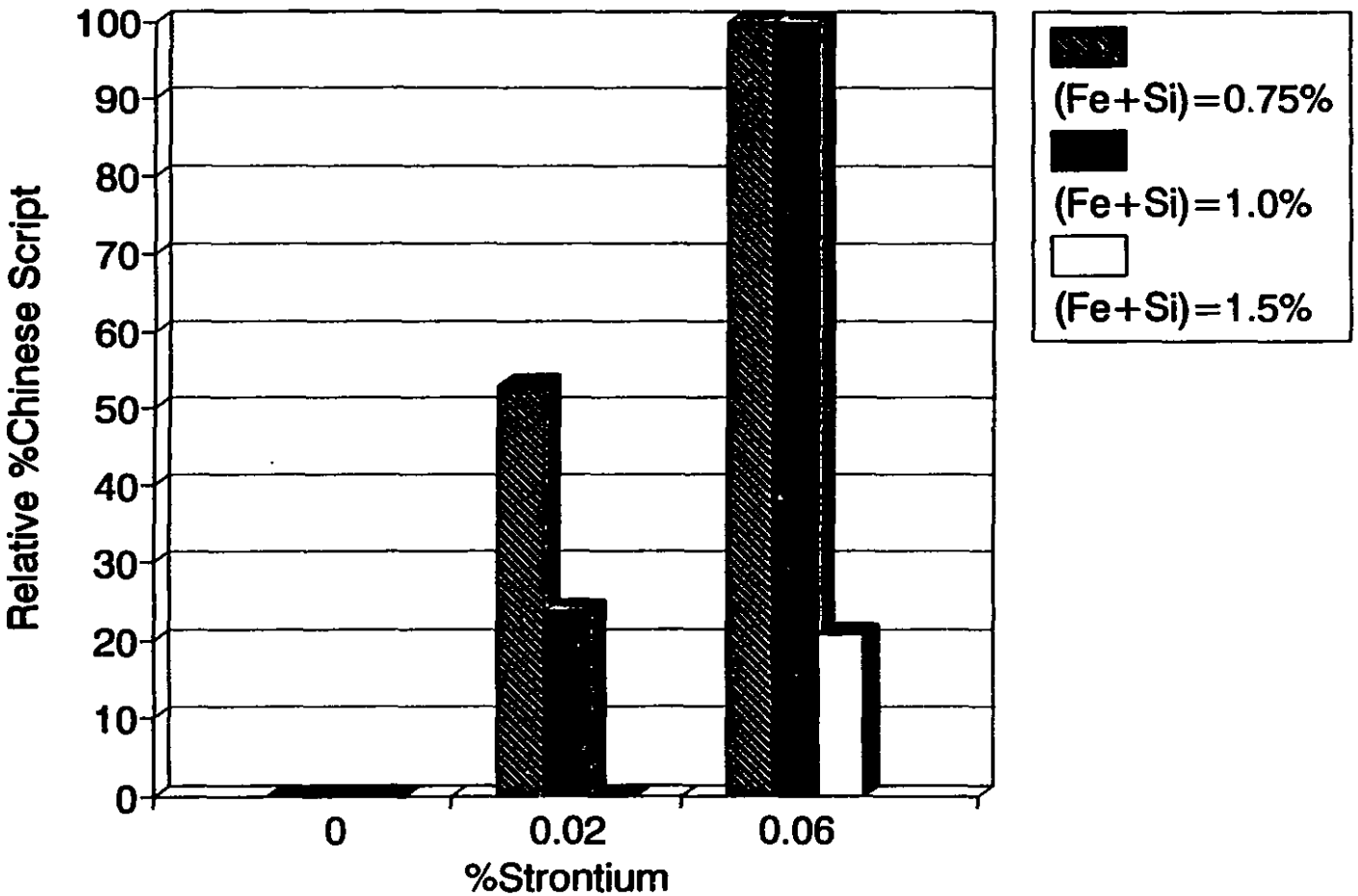

the lower (Fe+Si) totals caused all of the intermetallics in the microstructure to form as Chinese Script. The 0.06 weight percent strontium addition did promote Chinese Script formation in the alloy with the (Fe+Si) total of 1.5 percent, however, only 20.6 percent of the intermetallics formed as Chinese Script. A further addition of strontium could possibly cause more α-Chinese Script to form in this alloy. The optical micrographs presented in figure 4.10 show the effect of strontium modification on the microstructure for an alloy with an Fe/Si of 0.5 and cooling rate of 7°C/s. The microstructure of the strontium-free alloy contains only β-AlFeSi type intermetallic particles (fig 4.10a). An addition of 0.02 weight percent strontium to the alloy leads to a mixture of β-AlFeSi and α-AlFeSi particles with 53 percent being the α-AlFeSi phase (fig 4.10b). Further addition of strontium (0.06 weight pct.) caused all the intermetallic phase in the microstructure to form as α-Chinese Script as seen in figure 4.10c. The tendency for strontium to promote α-Chinese Script formation is also found for higher Fe/Si ratios.

The sole exception to this trend occurs in the alloy with (Fe+Si) of 1.5 weight percent, Fe/Si of 2.0 solidified at a rate of 7°C/s. Without strontium, the intermetallics in the microstructure consisted of 51.9 percent Chinese Script (however, this Script was found to be made up of the ternary α-AlFeSi and a binary Al-Fe phase). The addition of 0.02 weight percent strontium to this alloy did not cause more Chinese Script to form. A slight increase in relative percent Script (58.7 percent formed as Script) was observed with an addition of 0.06 percent strontium, however this increase is not statistically significant. Further strontium additions to this alloy could possibly promote larger amounts of the intermetallics to form with Chinese Script morphology. The scope of the

present work does not incorporate the effect of manganese additions since this would require a large number of controlled experiments.

Table 4.4 Relative Percent Chinese Script for Strontium Additions

wt% (Fe+Si)	Fe/Si	Rate (°C/s)	no Sr	0.02%Sr	0.06%Sr
0.75	0.5	1	0	6.4	70.8
		2	0	38.7	84.2
		7	0	53.0	100
0.75	1.0	1	88.0	100	100
		2	100	100	100
		7	100	100	100
0.75	1.5	1	100	100	100
		2	100	100	100
		7	100	100	100
0.75	2.0	1	100	100	100
		2	100	100	100
		7	100	100	100
1.0	0.5	1	0	0	89.4
		2	0	7.5	100
		7	0	23.7	100
1.0	1.0	1	33.6	67.6	73.2
		2	58.3	82.2	93.0
		7	63.7	100	100
1.0	1.5	1	57.3	100	100
		2	100	100	100
		7	100	100	100
1.0	2.0	1	92.5	100	100
		2	100	100	100
		7	100	100	100
1.5	0.5	1	0	0	16.3
		2	0	0	15.8
		7	0	0	20.6
1.5	1.0	1	29.4	45.4	36.1
		2	61.2	80.9	90.8
		7	100	100	100
1.5	1.5	1	64.7	73.5	94.4
		2	100	100	100
		7	100	100	100
1.5	2.0	1	75.9	100	100
		2	100	100	100
		7	51.9	52.9	58.7

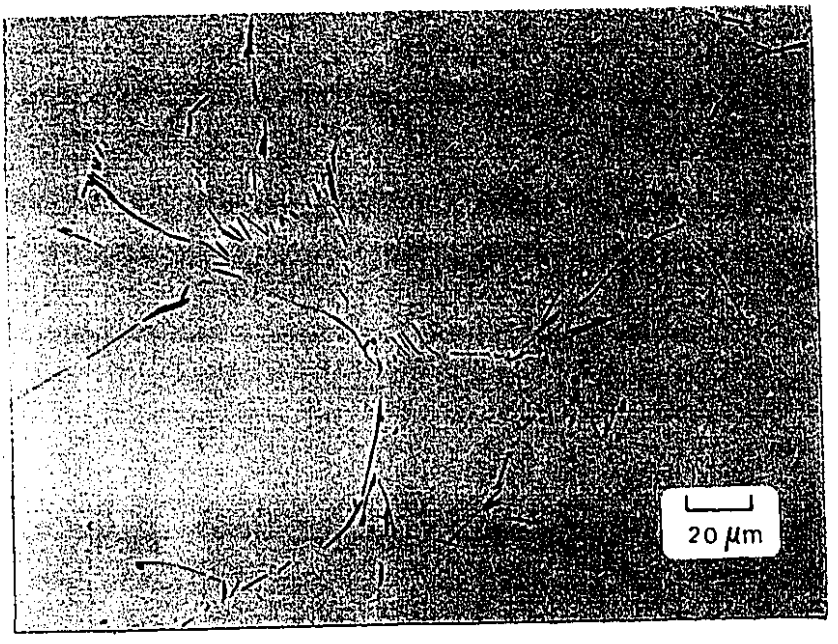

(a) no Sr

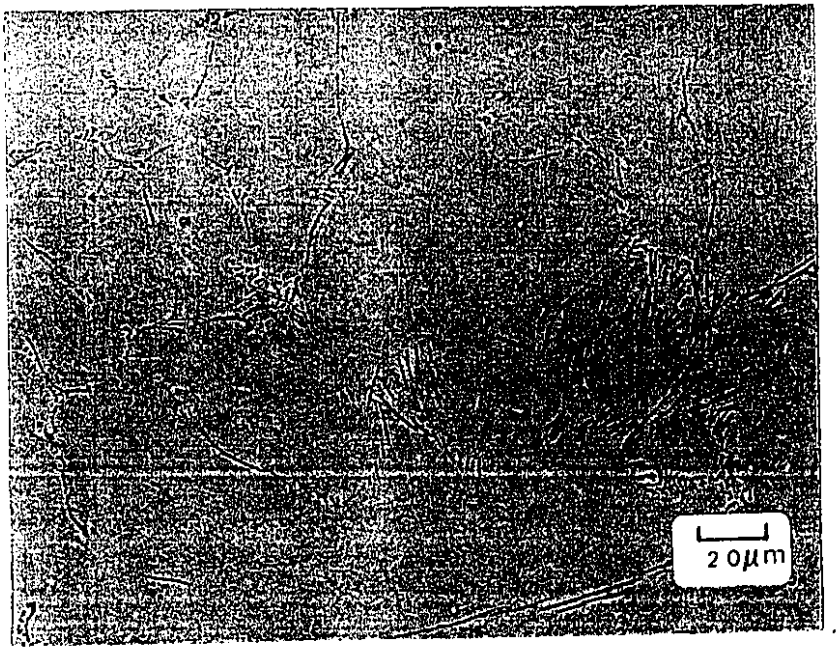

(b) 0.02 %Sr

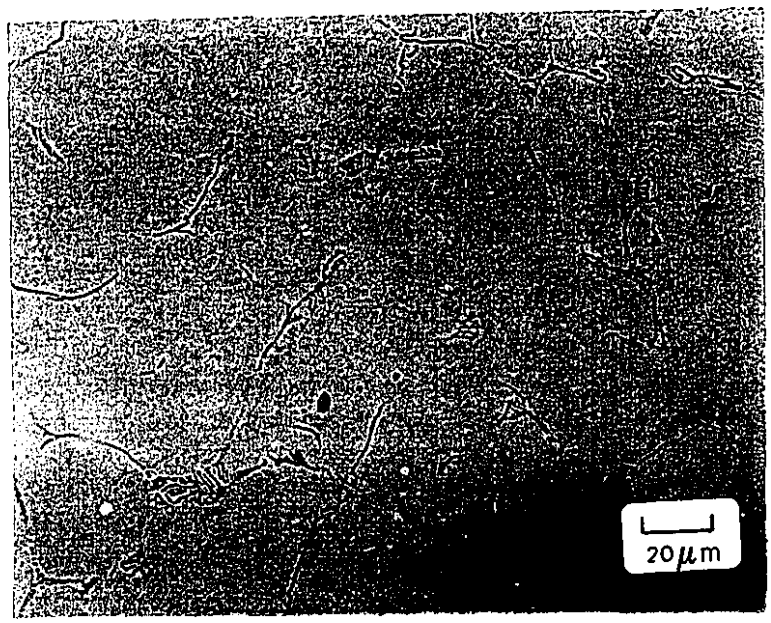

(c) 0.06 %Sr

Figure 4.10 Micrographs showing effect of strontium addition

4.1.2 Rolled Microstructures

In the samples that were rolled, the intermetallic particles were broken into small pieces for which it was impossible to identify the phases through optical microscopy. The size of the particles produced during rolling could greatly affect the mechanical properties of the metal sheet. The intermetallic particles for selected samples were sized and quantified to determine if the morphology of the as-cast intermetallics has any effect on the size of the particles created during rolling. Six samples with a constant (Fe+Si)

of 1.0 percent were analyzed, half of which contained no Chinese Script (i.e. 100 percent plate-like morphology) and the other half consisted only of intermetallics with the Chinese Script morphology in the as-cast structure. The particle size distribution results are listed in table 4.5 and are plotted in figure 4.11.

Table 4.5 Particle Size Distribution in Rolled Samples

Area (mic^2) Range	100% Plate-like morphology in as-cast[a]	100% Chinese Script in as-cast[b]
0 - 1	55.5 ± 2.8	56.6 ± 2.4
1 - 2	20.6 ± 3.2	22.4 ± 1.1
2 - 3	10.0 ± 1.6	8.7 ± 0.6
3 - 4	5.7 ± 1.1	4.6 ± 0.2
4 - 5	3.1 ± 1.1	3.1 ± 0.5
> 5	5.1 ± 1.8	4.7 ± 0.7

(a) average of 3 samples: #2, #3 and #11
(b) average of 3 samples: #53, #62 and #71

The results indicate that the particle size distributions of rolled samples are similar regardless of the morphology of the intermetallic phase in the as-cast microstructure. Over 75 percent of the particles were less than 2 mic^2 in area and approximately 5 percent of the particles were greater than 5 mic^2. Particles greater than about 5 mic^2 are generally considered detrimental to the mechanical properties, in particular the formability, of this type of metal sheet.

Figure 4.11 Particle Size Distribution
(on rolled samples)

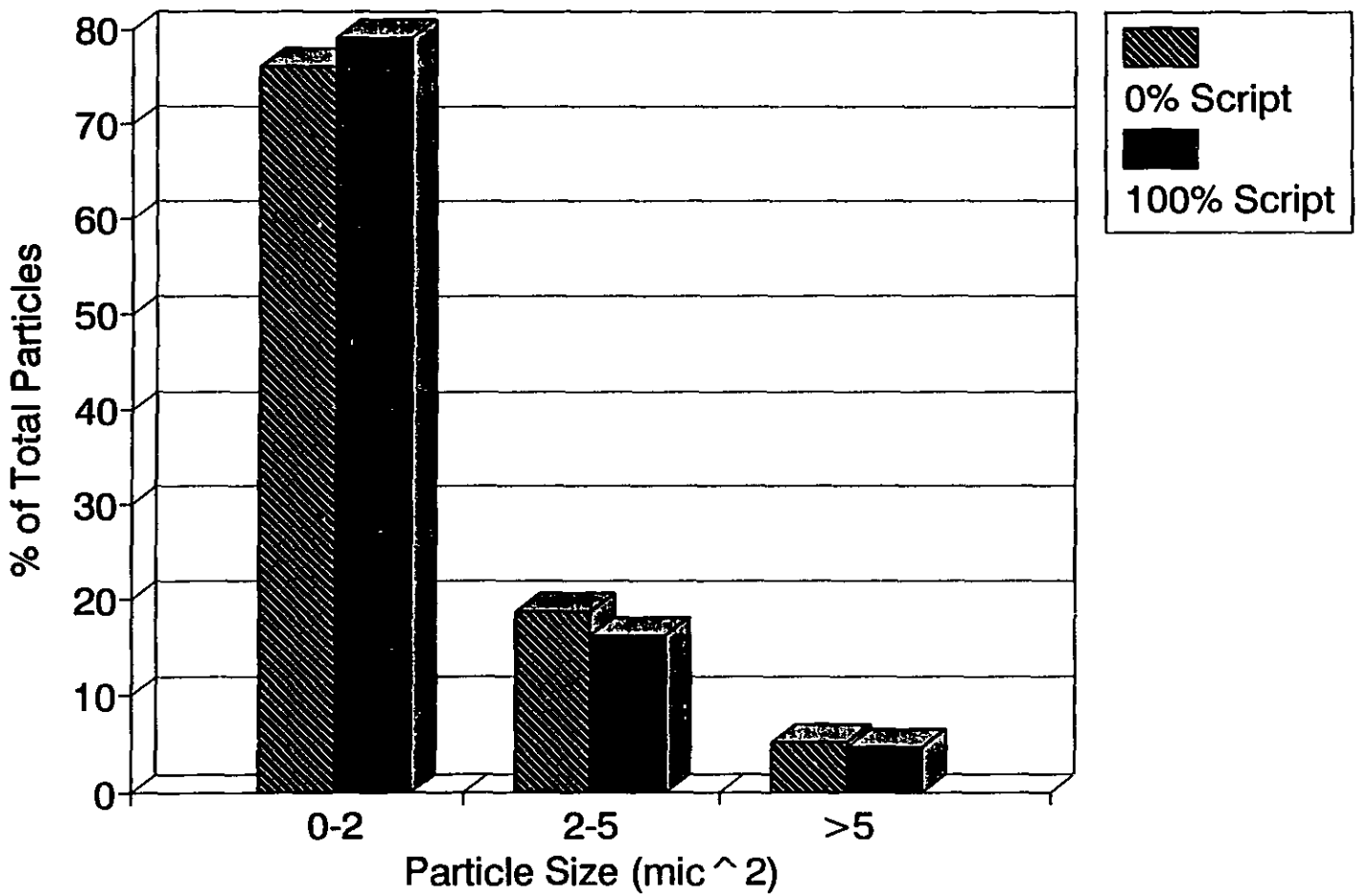

4.2 PART II: MECHANICAL TESTING

The intermetallic phases in the as-cast microstructures were quantified and particle size distributions were performed on the rolled microstructures in part I of this chapter. This second part attempts to relate the as-cast microstructure to the final mechanical properties and formability of the worked product as measured by tensile testing and Erichsen ball punch deformation tests.

4.2.1 Tensile Properties

Four tensile specimens were extracted for each rolled alloy. A complete list of the tensile results including the ultimate tensile strength (UTS), yield strength (YS) and percent elongation are given in Appendix B. A few tensile results are missing due to deficiencies in the rolling process. The ranges and average standard deviations for these results are listed in table 4.6 below.

Table 4.6 Summary of tensile results on rolled alloys

Tensile Property	Range	Average Standard Deviation
Tensile Strength	76.4 - 121.2 MPa	1.1 MPa
Yield Strength	32.2 - 48.7 MPa	3.0 MPa
Elongation	35.6 - 46.3 %	1.9 %

Figure 4.12 is a plot of the tensile properties versus the percent Chinese Script in the intermetallics for the entire set of alloys with an (Fe+Si) total of 1.0 percent. There is an increase in tensile strength as the relative amount of Chinese Script increases. In alloys containing only needles (i.e. 0% Chinese Script), the tensile strength is about 85 MPa. However, the tensile strength increases to approximately 100 MPa when the microstructure consists only of Chinese Script intermetallics. This is an increase in tensile strength of 18 percent which is significant. However, there is no significant change in percent elongation. The samples with no Chinese Script have an average elongation of 37 percent while the samples whose intermetallic phase consists only of Chinese Script have an average percentage elongation of 38 percent. This cannot be considered significant since the standard deviations for the elongation are in the order of 2.0 percent. This behaviour is difficult to explain, however it must be kept in mind that while the data in figure 4.12 is for a constant (Fe+Si) total of 1.0 wt%, the other parameters of these samples vary (i.e. Fe/Si ratio and cooling rate).

However, an increase in tensile strength may not necessarily be beneficial for these types of alloys. Some of the 1000 series alloys have maximum tensile strength limits, as listed in table 4.7 for three 1000 series standard alloys.

Table 4.7 Mechanical property limits - Sheet and Plate[1]

Alloy(1)	UTS(2) (MPa) Minimum	Maximum
1060	55.2	96.5
1100	75.8	106.9
1350	55.2	96.5

(1) annealed condition
(2) valid for specified thickness: 0.15-76.2mm

Figure 4.13 presents the tensile strength results for all three (Fe+Si) totals. At the highest level of (Fe+Si), there is no significant change in tensile strength as the morphology of the intermetallic phase changes. It is difficult to determine if there is a change in tensile strength at the lower level of (Fe+Si) because most of the samples at this level (i.e. 0.75 percent) consisted only of Chinese Script. However, there does not appear to be a significant difference between the samples with 50 and 100 percent Chinese Script at (Fe+Si) of 0.75 weight percent. The percentage elongation results for the (Fe+Si) totals of 0.75 and 1.5 percent were similar to those of the 1.0 percent in that there was no significant change in elongation with a change in the morphology of the intermetallic phase.

By comparing the three levels of (Fe+Si), it can be seen that the tensile strength increases with increasing (Fe+Si) total. For samples containing 100 percent Chinese Script, the average tensile strength is about 85 Mpa at 0.75 wt%, 100 MPA at 1.0 wt% and increases further to about 110 MPa at 1.5 wt% (Fe+Si). This increase in strength with (Fe+Si) total is probably due mainly to solid solution strengthening as the impurity level increases.

Fig. 4.12 Tensile Properties vs %Script
(Fe+Si)= 1.0 wt%

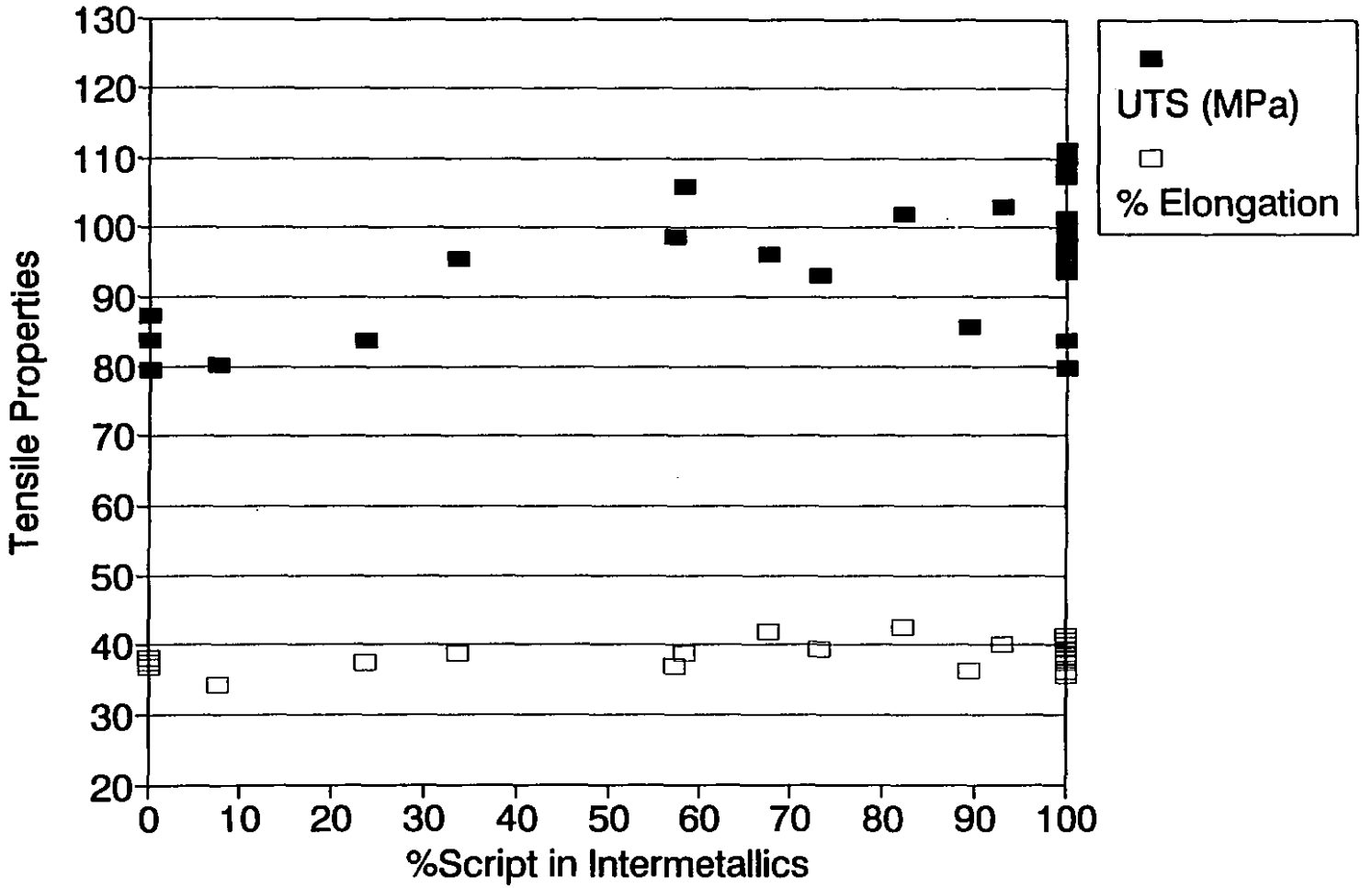

Figure 4.13 Tensile Results vs %Script
For All Alloys

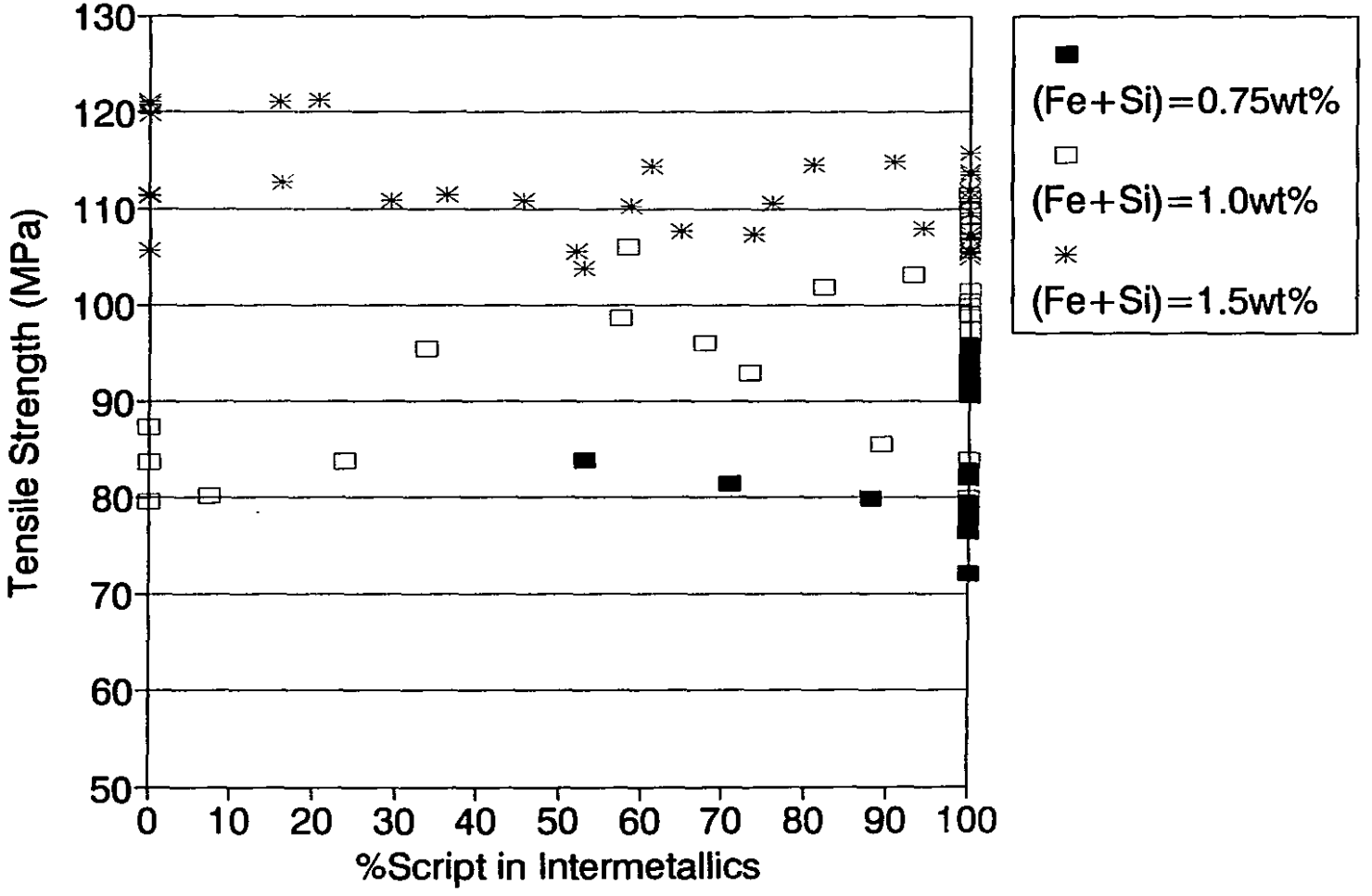

Figure 4.14 Elongation vs %Script
For All Alloys

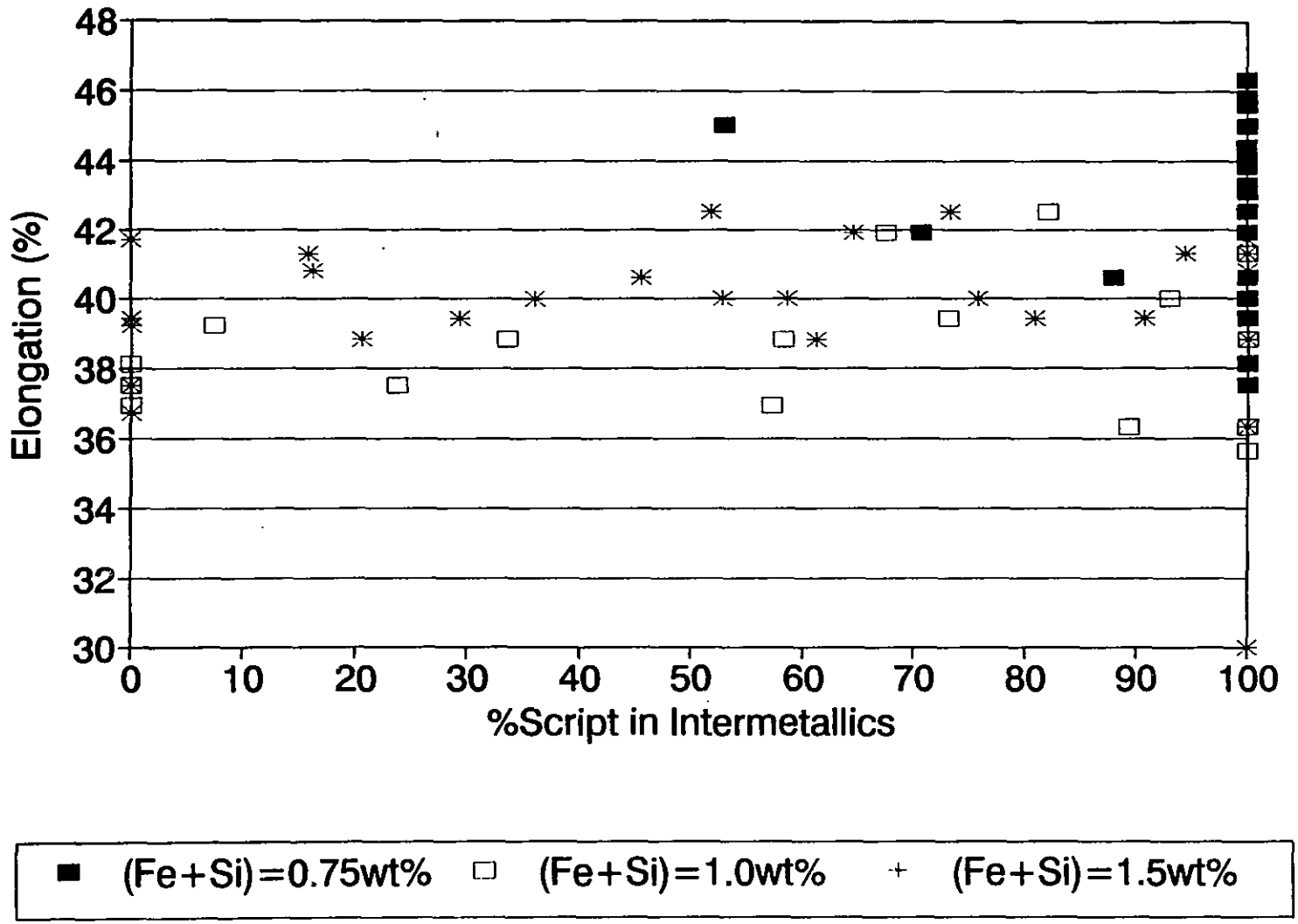

4.2.2 Formability Testing

Six Erichsen ball punch deformation tests were performed on each rolled alloy to obtain a measure of formability. As the height of the cup formed prior to fracture increases, the formability of the sheet also increases. The complete list of these results is given in Appendix B.

The plots of Erichsen cup height versus the percent Chinese Script in the as-cast microstructure for the three (Fe+Si) levels of 0.75, 1.0 and 1.5 weight percent are shown in figures 4.15, 4.16 and 4.17 respectively. All three graphs show a slight increase in the formability of the sheet metal with increasing relative percent Chinese Script in the as-cast structure. However, the increase in Erichsen cup height is in the order of 0.5mm which is not a very significant increase (about 5 percent) [28]. Table 4.8 lists the average Erichsen values for the alloys containing 0 and 100 relative percent Chinese Script morphology for the three (Fe+Si) levels.

Table 4.8 Erichsen Results

Relative % Script	Height of Erichsen Cup (mm)		
	(Fe+Si)= 0.75 wt%	(Fe+Si)= 1.0 wt%	(Fe+Si)= 1.5 wt%
0	9.5 ± 0.1	9.4 ± 0.1	9.2 ± 0.2
100	9.9 ± 0.2	9.9 ± 0.2	9.7 ± 0.2

The formability results for the (Fe+Si) levels of 0.75 and 1.0 percent are similar, however the formability of the alloys with the highest (Fe+Si) of 1.5 weight percent is slightly lower, as shown in table 4.8. Again, the difference is probably not significant.

Figure 4.15 Formability Results
(Fe+Si) = 0.75 wt%

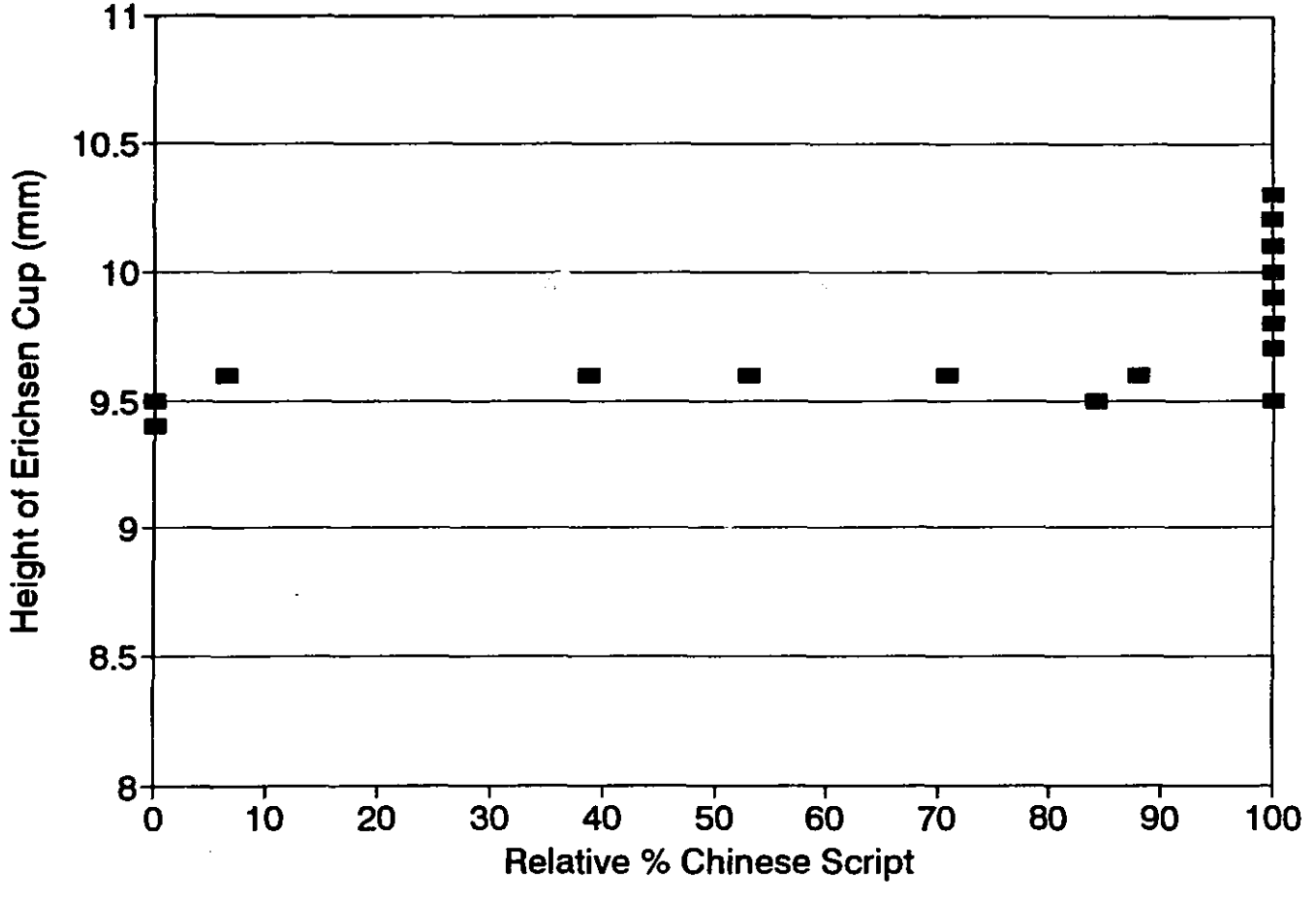

Figure 4.16 Formability Results
(Fe+Si) = 1.0 wt%

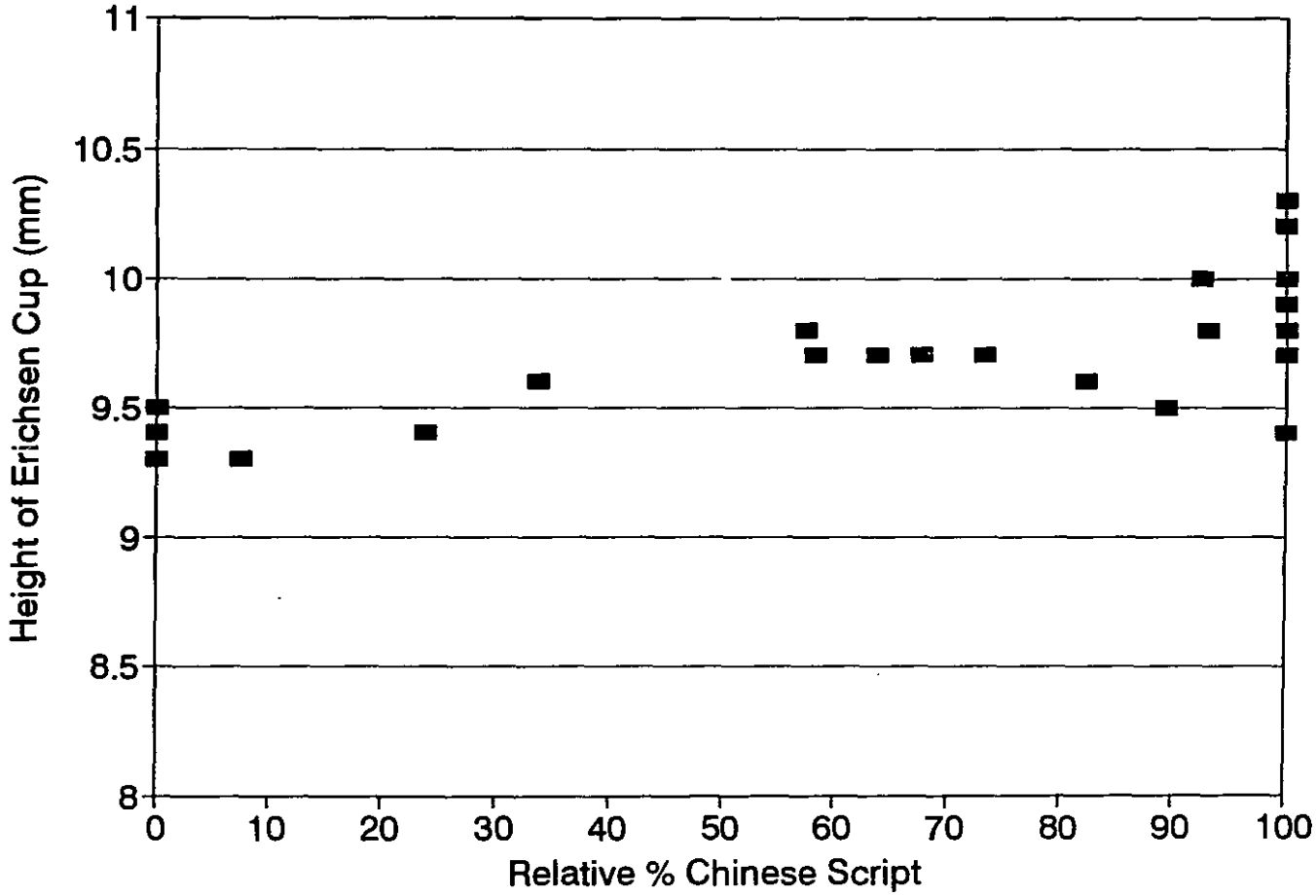

Figure 4.17 Formability Results
(Fe+Si) = 1.5 wt%

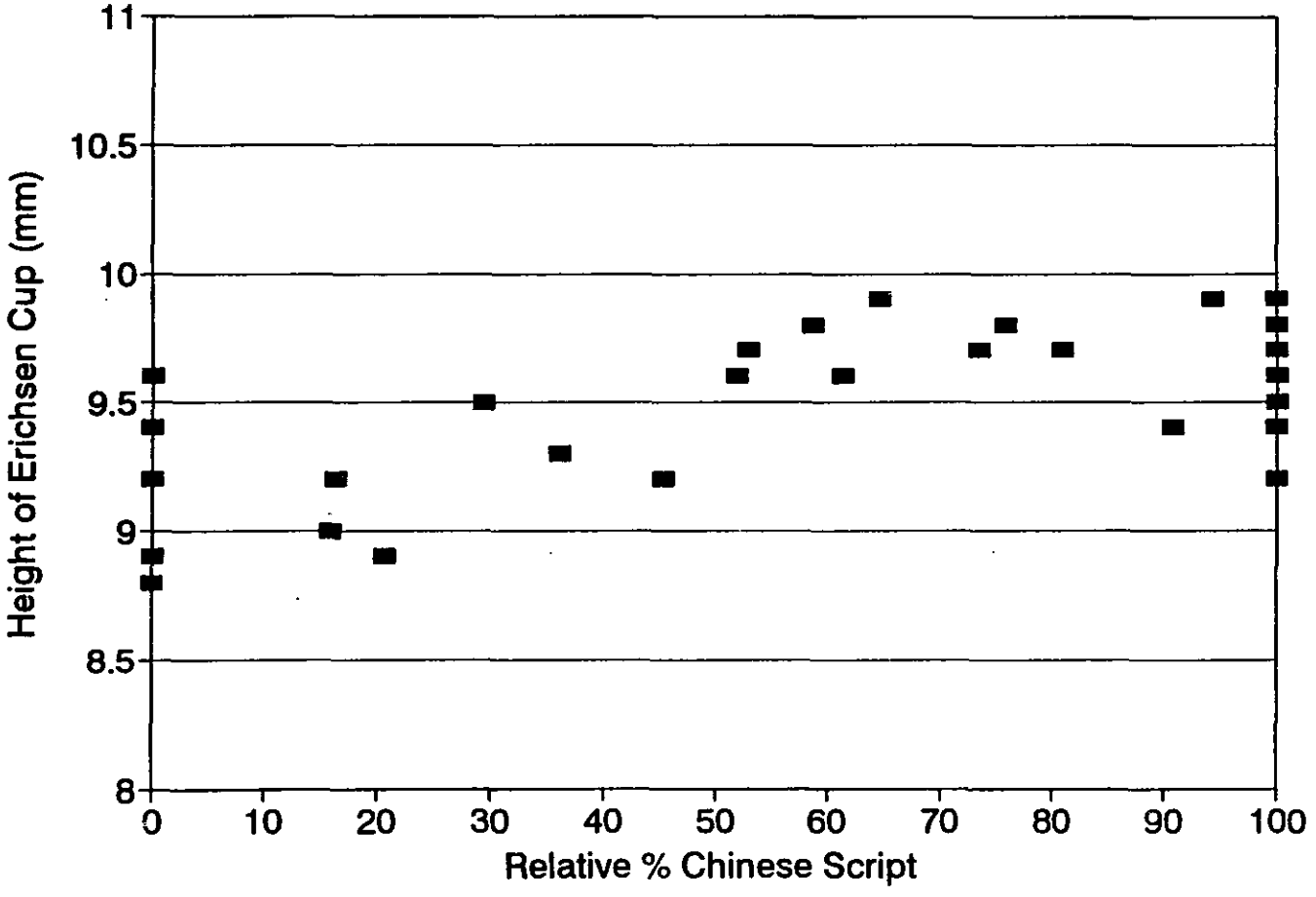

In the first part of the study, the conditions at which the Chinese Script morphology forms naturally during ingot solidification (i.e. increasing cooling rates and Fe/Si ratios) were determined for the 1000 series of wrought aluminum alloys. The addition of strontium to the melt was also found to promote Chinese Script formation in the cast microstructure.

In the second part of the study, it was determined that the presence of the Chinese Script morphology in the as-cast structure has no beneficial effect on the formability of the worked product. This can be explained by looking at the particle distribution results of the rolled aluminum. These results showed that the intermetallics broke into small pieces during rolling for which the particle size distribution was similar, regardless of the morphology of the intermetallics in the as-cast structure. Therefore, the Erichsen deformation results showed no difference in formability.

The 1000 series consists mainly of rolling alloys, however some of the alloys in the 1000 series are extruded. In this case, the morphology of the Al-Fe-Si intermetallic phases would probably have a more significant effect on the final product, as was found in the 6000 series (mainly extrusions alloys) [23]. In extrusions, it is the as-cast metal which is extruded to directly produce the final product, whereas products made from rolled material are manufactured after the rolling process itself when the intermetallics have already been fragmented.

The maximum (Fe+Si) limit in the 1000 series of alloys registered with the Aluminum Association is 1 weight percent. The alloys with an (Fe+Si) level 50 percent higher than this (i.e. 1.5 wt pct.) were not found to be significantly less formable than the alloys with lower (Fe+Si) levels, as measured by the Erichsen ball punch deformation tests. However, these alloys with the high impurity level of 1.5 weight percent (Fe+Si) were found to have tensile strengths above the maximum limits set by the Aluminum Association.

CHAPTER
5

MAIN CONCLUSIONS

5.1 QUANTITATIVE METALLOGRAPHY

The first part of this study consisted of experimentally determining how the type and quantity of intermetallic phases in the cast microstructure varies with chemical composition and solidification rate. The following main conclusions can be drawn from this study:

1 - Two main ternary Al-Fe-Si intermetallic phases were found to form in the synthetic alloys that were produced to simulate the 1000 series of wrought aluminum alloys. They are: the acicular β-AlFeSi phase (Al_5FeSi) which appears as needles in section, and the α-AlFeSi phase (Al_8Fe_2Si) which has the well-known Chinese Script morphology.

2 - As the Fe/Si ratio increases, there is a strong tendency for the α-AlFeSi Chinese Script phase to form.

3 - For a given Fe/Si ratio, there is a strong tendency for α-Chinese Script phase formation as the cooling rate increases.

4 - In alloys containing more silicon than iron (i.e. Fe/Si < 1), only the acicular β-AlFeSi phase is formed regardless of the cooling rate.

5 - For a given Fe/Si ratio and cooling rate, there is a tendency for more Si-rich particles (β-AlFeSi) to form as the (Fe+Si) alloying content increases.

6 - The addition of strontium promotes the formation of α-AlFeSi Chinese Script for the different Fe/Si ratios, cooling rates and (Fe+Si) totals.

7 - The size distributions of the particles produced during rolling are similar regardless of the morphology of the intermetallic phase in the as-cast structure.

5.2 MECHANICAL PROPERTIES

The second part of this study was an attempt to relate the as-cast structure to the mechanical properties of the wrought product (sheet metal). The mechanical testing consisted of tensile testing and formability testing using the Erichsen ball punch deformation test. The following conclusions can be drawn from this second part of the study:

8 - For an (Fe+Si) total of 1.0 weight percent, the tensile strength increased with increasing relative percent Chinese Script in the rolled microstructure. However, no

significant change in percent elongation was observed with the different morphologies of the intermetallic phase.

9 - An increase in tensile strength was observed with increasing (Fe+Si) levels, probably due to solid solution strengthening.

10 - The formability of the sheet metal (as measured by the Erichsen cup test) was found to increase slightly (approx. 5 percent increase) by increasing the relative percentage Chinese Script in the as-cast structure from 0 to 100 percent, for all three (Fe+Si) levels.

11 - The alloys with the highest (Fe+Si) level of 1.5 weight percent were found to be slightly less formable (approx. 5 percent lower) than the alloys with the lower (Fe+Si) levels.

REFERENCES

1. "Aluminum standards and data 1988", Aluminum Association Inc., Ninth Ed., July 1988, pp 97 & 103.

2. "Aluminum: Properties and Physical Metallurgy", John E. Hatch, American Society for Metals, Ohio, 1984, pp 355-358.

3. Y. Langsrud, Silicon in commercial aluminum - What becomes of it during DC-casting?, Key Eng. Materials, Vols 44-45, 1990, pp 95-116.

4. J. Lendvai, The structure of DC cast Al-Fe and Al-Fe-Si alloys, Materials Science Forum, Vol 13, 1987, pp 101-118.

5. L. F. Mondolfo, Aluminum alloys - Structure and properties, Butterworths, London, 1976.

6. G. Phragmen, J. Inst. Metals, Vol 77, 1950, pp 489.

7. A. Griger, V. Stefaniay, A. Lendvai and T. Turmezey, Z. Metallkunde, Vol 65, 1989, pp 1049-1057.

8. A. L. Dons, AlFeSi-Particles in industrially cast aluminum alloys, Z. Mettalkunde, Vol 76, 1985, pp 609-612.

9. I. Miki, H. Kosuge and K. Nagahama, J. Jap. Inst. Light Metals, Vol 32, 1975, pp 1.

10. R. M. K. Young and T. W. Clyne, Scripta Metallurgica, Vol 15, 1981, pp 1211-16.

11. E.H. Hollingsworth, G.R. Frank and R.E. Willett, Trans. Met. Soc. AIME, Vol 224, 1962, pp 188.

12. I. Miki, H. Kosuge and K. Nagahama, J. Jap. Inst. Light Metals, Vol 25, 1975, pp 1-9.

13. H. Kosuge and I. Mizukami, J. Japan Inst. Light Metals, Vol 25, 1975, pp 48-58.

14. H. Westengen, Formation of intermetallic compounds during DC casting of a commercial purity Al-Fe-Si alloy, Z. Mettalkunde, Vol 73, 1982, pp 360-368.

REFERENCES

15. C.Y. Sun and L.F. Mondolfo, J. Inst. Metals, Vol 95, 1967, pp 384.

16. C.J. Simensen and R. Vellasamy, Z. Metallkde, Vol 68, 1977, pp 428.

17. D. Munson, J. Inst. Metals, Vol 95, 1967, pp 217-219.

18. A. L. Dons, Z. Mettalkunde, Vol 75, 1984, pp 170.

19. V. Bischofberger, G. Neite and H.E. Exner, Key Engineering Materials, Vols 44 & 45, p 333, 1990.

20. M. C. Hanna, S. Z. Lu, A. Hellawell, Metall. Trans., Vol 15A, 1986, pp 459-469.

21. B. Closset, J. E. Gruzleski, Metall. Trans., Vol 13A, 1984, pp 945-951.

22. B. Lee Tuttle, Proc. Int. Molten Aluminum Processing Conf., AFS, 1986, pp 31.

23. M. H. Mulazimoglu, B. Closset and J. E. Gruzleski, Evaluation of the metallurgical effects of strontium on cast 6000 series aluminum alloys, Aluminum, Vol 68, 1992, pp 489-492.

24. L. R. Morris and F. B. Miners, U.S. patent, No. 392 6690, 1975.

25. ASTM Designation: E 643- 84 (Reapproved 1990)

26. T. Turmezey, AlFe and AlFeSi Intermetallic phases in aluminum alloys, Materials Science Forum, Vol 13, 1987, pp 121-132.

27. Per Skjerpe, Intermetallic phases formed during DC-casting of an Al-0.25 wt pct Fe-0.13 wt pct Si alloy, Metallurgical Transactions, Vol 18A, 1987, pp 189-199.

28. Personal contact with mechanical testing laboratory at Alcan Kingston Research & Development Centre.

APPENDIX A
Quantitative Metallography Data

(Fe+Si) = 0.75 wt%

Sample #	Area-B (mic) ^ 2	%Beta	Area-A (mic) ^ 2	%Alpha	TOTAL AREA	%Inter-metallics	Relative %Beta	Relative %Alpha
131	488.4	1.05	33.15	0.07127	521.55	1.1	93.6	6.4
132	543.4	1.168	342.9	0.7374	886.3	1.9	61.3	38.7
133	343	0.7375	386.9	0.8319	729.9	1.6	47.0	53.0
141	353.4	0.76	856.6	1.842	1210	2.6	29.2	70.8
142	133.8	0.2876	714.7	1.537	848.5	1.8	15.8	84.2
151	178.4	0.3835	1307	2.811	1485.4	3.2	12.0	88.0
152	0	0	543.8	1.169	543.8	1.2	0.0	100.0
					Avg (%)	1.9		
					STD Dev	0.7		

(Fe+Si) = 1 wt%

11	993.7	2.137	18.34	0.03943	1012.04	2.2	98.2	1.8
12	891.9	1.918	71.83	0.1544	963.73	2.1	92.5	7.5
13	652	1.402	202.6	0.4357	854.6	1.8	76.3	23.7
21	104.1	0.2238	882.4	1.897	986.5	2.1	10.6	89.4
22	0	0	1064	2.288	1064	2.3	0.0	100.0
31	765.7	1.646	387.4	0.833	1153.1	2.5	66.4	33.6
32	689	1.481	963.9	2.072	1652.9	3.6	41.7	58.3
33	549.1	1.181	965.5	2.076	1514.6	3.3	36.3	63.7
41	590.5	1.27	1230	2.646	1820.5	3.9	32.4	67.6
42	259.9	0.5587	1199	2.577	1458.9	3.1	17.8	82.2
51	477.3	1.026	1302	2.799	1779.3	3.8	26.8	73.2
52	127.5	0.2741	1686	3.625	1813.5	3.9	7.0	93.0
61	521.2	1.2383	699.7	1.6617	1220.86	2.9	42.7	57.3
91	108.3	0.233	135	2.871	243.3	3.1	7.5	92.5
					Avg(%)	2.9		
					STD Dev	0.7		

(Fe+Si) = 1.5 wt%

Sample #	Area-B (mic) ^ 2	%Beta	Area-A (mic) ^ 2	%Alpha	TOTAL AREA	%Inter-metallics	Relative %Beta	Relative %Alpha
291	1033	2.222	201.4	0.433	1234.4	2.7	83.7	16.3
292	1587	3.412	296.8	0.6381	1883.8	4.1	84.2	15.8
293	1144	2.46	296.5	0.6375	1440.5	3.1	79.4	20.6
301	2098	4.51	872.2	1.875	2970.2	6.4	70.6	29.4
302	943.7	2.029	1491	3.205	2434.7	5.2	38.8	61.2
311	995	2.139	831.9	1.789	1826.9	3.9	54.5	45.5
312	470.9	1.013	1991	4.281	2461.9	5.3	19.1	80.9
321	1560	3.354	882.4	1.897	2442.4	5.3	63.9	36.1
322	261.5	0.5623	2570	5.526	2831.5	6.1	9.2	90.8
331	833.1	1.791	1524	3.277	2357.1	5.1	35.3	64.7
341	667.5	1.435	1850	3.978	2517.5	5.4	26.5	73.5
351	117.5	0.2527	1984	4.266	2101.5	4.5	5.6	94.4
361	622.7	1.339	1962	4.219	2584.7	5.6	24.1	75.9
362	0	0	3559	7.653	3559	7.7	0.0	100.0
363	1624	3.492	1753	3.769	3377	7.3	48.1	51.9
371	29.06	0.06249	2643	5.682	2672.06	5.7	1.1	98.9
373	1048	2.253	1177	2.531	2225	4.8	47.1	52.9
383	1139	2.449	1622	3.487	2761	5.9	41.3	58.7
					Avg (%)	5.2		
					STD Dev	1.3		

APPENDIX B
Mechanical Testing Data

TENSILE RESULTS

Sample #	UTS (MPa)	Std. Dev. (MPa)	YS (MPa)	Std. Dev. (MPa)	Elong. (%)	Std. Dev. (%)
2	87.3	1.7	39.1	3.5	38.1	2.1
3	85.5	1.4	41.1	2.8	36.3	1.2
11	83.7	1.2	37.1	3.0	36.9	2.1
12	80.1	1.1	36.3	3.6	36.4	3.7
13	79.8	1.6	37.9	5.1	38.1	2.1
21	79.5	1.3	46.9	3.5	37.5	2.5
22	83.7	1.0	40.6	1.9	37.5	1.8
23	84.2	1.5	42.4	3.6	36.3	2.8
31	95.4	0.8	39.8	2.8	38.8	1.2
32	96.0	1.4	48.0	3.7	41.9	2.1
33	93.0	2.2	39.1	2.5	39.4	1.1
41	105.9	2.0	45.3	4.0	38.8	1.2
42	101.9	3.1	44.9	3.7	42.5	1.8
43	103.0	1.9	37.1	2.0	40.0	1.8
52	98.9	2.1	40.0	4.1	37.5	1.8
53	95.4	1.9	41.0	2.0	39.4	2.7
61	98.6	1.5	41.0	3.9	36.9	2.1
62	95.4	2.0	35.2	0.0	37.5	4.0
63	99.1	1.5	42.0	1.7	39.4	2.7
71	94.2	2.2	44.9	4.2	40.6	2.1
72	93.5	1.7	36.1	1.7	35.6	4.2
73	100.3	1.5	46.9	3.8	40.0	0.0
82	111.3	1.2	47.9	4.7	41.3	1.3
83	101.3	1.7	37.1	4.9	38.1	2.7
92	109.2	1.8	42.0	4.3	40.6	2.7
93	110.0	1.9	37.1	2.0	40.0	1.8
101	107.7	1.6	32.2	3.2	35.6	3.2
102	107.7	3.1	40.0	4.3	39.4	1.1
103	107.5	1.4	37.1	2.0	39.4	1.1
111	83.8	1.5	39.1	1.6	38.1	2.7
112	97.4	2.0	48.4	2.7	38.8	2.8
113	94.3	1.2	48.0	1.3	36.3	2.2
123	81.4	1.4	39.1	1.9	41.9	2.1
142	83.8	1.9	43.4	4.9	45.0	1.8
143	79.2	1.6	38.3	3.2	43.8	2.8
151	79.8	0.7	41.0	5.1	40.6	2.7
152	78.2	1.9	38.3	6.2	43.1	2.7
153	76.4	0.7	32.6	1.3	46.3	1.3

TENSILE RESULTS
(continued)

Sample #	UTS (MPa)	Std. Dev. (MPa)	YS (MPa)	Std. Dev. (MPa)	Elong. (%)	Std. Dev. (%)
161	82.7	1.9	42.6	7.0	44.4	1.1
162	77.8	1.1	36.7	1.7	41.9	2.1
163	82.0	1.1	39.8	2.8	40.6	2.7
171	79.3	1.0	38.3	4.6	39.4	2.7
172	78.9	1.1	40.2	5.2	40.0	1.8
173	79.4	0.8	45.7	6.7	38.1	2.1
182	82.4	1.7	42.2	5.2	37.5	1.8
191	94.0	0.4	45.3	4.3	44.4	1.1
192	94.2	0.7	42.4	3.4	43.8	2.8
193	95.6	0.9	38.1	3.0	42.5	0.0
201	92.6	0.3	39.4	3.6	45.8	1.2
202	94.7	0.3	39.5	1.1	45.0	0.0
203	95.7	1.4	39.1	1.3	44.4	1.1
241	91.1	0.0	38.0	0.7	43.8	4.3
242	90.6	0.6	36.3	0.7	43.8	1.2
243	91.7	0.7	35.4	0.6	45.8	2.4
251	92.7	0.8	37.8	2.5	43.3	2.4
252	94.6	0.6	38.6	1.6	45.6	2.7
253	93.9	0.9	37.8	1.1	45.0	2.5
261	92.7	0.6	38.9	2.6	43.8	1.2
262	93.7	0.5	38.7	1.1	43.3	2.4
263	92.7	0.4	42.7	5.1	44.2	2.4
271	111.3	0.5	44.0	4.8	41.7	2.4
272	111.5	0.8	44.5	8.9	37.5	2.5
273	112.6	0.3	45.4	2.0	40.8	1.2
281	120.8	1.2	45.2	1.9	36.7	1.2
282	119.8	1.0	45.4	4.5	39.2	1.2
283	121.1	1.8	44.7	2.0	41.3	1.3
291	121.0	1.2	44.5	3.5	39.4	1.1
292	120.7	1.4	45.6	2.1	37.5	1.8
293	121.2	0.3	45.7	1.1	38.8	1.2
301	110.8	0.6	46.7	1.7	39.4	1.1
302	110.9	0.9	44.4	4.1	40.6	2.1
303	111.5	0.2	46.7	2.9	40.0	0.0
311	114.4	0.7	44.1	5.2	38.8	2.8
312	114.5	0.7	48.7	2.2	39.4	1.1
313	114.8	1.1	44.9	5.3	39.4	1.1

TENSILE RESULTS
(continued)

Sample #	UTS (MPa)	Std. Dev. (MPa)	YS (MPa)	Std. Dev. (MPa)	Elong. (%)	Std. Dev. (%)
321	113.8	1.1	46.1	2.9	36.3	1.2
322	113.5	0.6	41.9	2.3	38.8	1.2
323	115.8	0.9	48.2	5.3	38.8	1.2
331	107.7	0.3	42.3	2.9	41.9	2.1
332	107.3	0.6	43.3	0.8	42.5	0.0
333	107.9	0.2	40.8	4.1	41.3	1.3
341	104.9	0.3	42.4	0.9	43.1	2.1
342	109.5	0.6	43.3	3.7	41.3	3.7
343	111.8	1.6	46.2	2.3	40.6	1.1
351	111.0	1.1	44.7	1.7	38.8	1.2
352	110.3	0.2	45.1	1.6	40.0	0.0
353	113.5	0.4	42.7	4.7	42.5	0.0
361	110.5	0.5	45.8	1.7	40.0	3.1
362	105.3	0.8	45.2	3.1	40.8	1.2
363	107.4	0.6	44.6	3.8	40.6	2.7
371	105.5	0.4	42.3	1.0	42.5	0.0
372	105.8	0.6	42.7	1.3	41.7	3.1
373	106.9	1.8	46.6	3.6	36.3	6.3
381	105.5	0.4	43.1	2.8	42.5	2.5
382	105.7	0.6	44.3	1.0	37.5	2.5
383	103.8	1.2	39.8	0.5	40.0	3.1

ERICHSEN FORMABILITY RESULTS
(Average of 6 tests per sample)

SAMPLE #	Height of Cup (mm)	Std. Deviation (mm)
1	9.5	0.2
2	9.4	0.1
3	9.5	0.1
11	9.3	0
12	9.3	0
13	9.4	0
21	9.4	0
22	9.4	0
23	9.4	0
31	9.6	0
32	9.7	0.1
33	9.7	0.1
41	9.7	0.1
42	9.6	0.1
43	9.8	0
51	9.7	0
52	9.7	0.1
53	9.7	0
61	9.8	0.1
62	9.8	0
63	9.9	0
71	9.8	0
72	10	0
73	10	0
81	10	0
82	9.9	0
83	9.9	0.1
91	10	0
92	9.8	0.2
93	10.2	0
101	9.8	0
102	9.8	0
103	10	0
111	9.9	0
112	10	0
113	10.3	0.1

ERICHSEN FORMABILITY RESULTS
(CONTINUED)

SAMPLE #	Height of Cup (mm)	Std. Deviation (mm)
121	9.5	0.1
122	9.6	0
123	9.6	0
131	9.5	0
132	9.6	0
133	9.5	0
141	9.4	0.1
142	9.6	0
143	9.5	0.1
151	9.6	0.2
152	9.7	0
153	9.7	0
161	9.7	0
162	9.7	0.1
163	9.8	0.1
171	9.8	0
172	9.8	0
173	9.8	0
181	not available	
182	not available	
183	not available	
191	10.1	0
192	10.2	0
193	10.1	0.1
201	10.3	0
202	10	0.1
203	10.1	0.1
241	10	0.1
242	9.9	0.1
243	10.1	0
251	10	0
252	10	0.1
253	10	0.1
261	10	0.1
262	10	0.1
263	10	0

ERICHSEN FORMABILITY RESULTS
(CONTINUED)

SAMPLE #	Height of Cup (mm)	Std. Deviation (mm)
271	9.4	0.1
272	9.6	0.3
273	9.2	0
281	9.4	0.1
282	9.2	0.1
283	9	0.2
291	8.9	0
292	8.8	0.1
293	8.9	0.1
301	9.5	0
302	9.2	0.1
303	9.3	0.1
311	9.6	0
312	9.7	0.1
313	9.4	0.1
321	9.4	0
322	9.5	0
323	9.2	0
331	9.9	0.1
332	9.7	0.1
333	9.9	0.1
341	9.7	0.2
342	9.8	0.1
343	9.7	0.2
351	9.6	0
352	9.6	0
353	9.8	0
361	9.8	0.1
362	9.8	0.1
363	9.9	0.1
371	9.9	0.1
372	9.8	0
373	9.8	0.1
381	9.6	0.1
382	9.7	0
383	9.8	0.1